

Nonradiative capture and recombination by multiphonon emission in GaAs and GaP

C. H. Henry and D. V. Lang

Bell Laboratories, Murray Hill, New Jersey 07974

(Received 27 May 1975)

Data are presented for 9 capture cross sections of deep levels in GaAs and 4 in GaP which can be interpreted as capture by multiphonon emission (MPE). At high temperatures the cross sections have the form $\sigma = \sigma_{\infty} e^{-E_{\infty}/kT}$ where $\sigma_{\infty} = 10^{-14} - 10^{-15} \text{ cm}^2$ and $E_{\infty} = 0 - 0.56 \text{ eV}$. A simple theory of MPE capture is presented in which vibrations of a single lattice coordinate modulate the depth of the potential well binding the carrier. In this model capture results from lattice vibrations causing the crossing of free- and bound-carrier levels. The breakdown of the adiabatic approximation near the crossing is discussed. The calculated cross sections have the form $\sigma = Af(0)$ where $f(h\nu)$ is the normalized line shape for radiative capture. The lattice relaxation properties of the center determine $f(0)$. The temperature dependence of $f(0)$ correctly accounts for the thermally activated behavior of the cross sections at high temperatures. Classical and quantum treatments of the lattice motion give the same expression for σ at high temperature. A detailed calculation of A is made for the capture of a carrier by an attractive neutral impurity in the case where both the free-carrier and bound-carrier wave functions are describable in a one-band effective-mass approximation. The theoretical value of A leads to $\sigma_{\infty} \approx 6 \times 10^{-15} \text{ cm}^2$, the same order of magnitude as the experimental values. However, many of the experimental cross sections involve complexities not accounted for in this simple model such as charged impurities and transitions between free states and bound states of different symmetry. The lattice relaxation parameters are experimentally determined for the Zn-O and O centers in GaP. Lattice relaxation is found adequate to explain the large cross sections for electron capture by the Zn-O center and hole capture by the two-electron state of O. The studies of the O and Zn-O centers also provide evidence for nonlinear changes in the impurity energy level with lattice displacement which decrease the electron capture cross sections and greatly enhance the hole recombination cross sections. The source of this nonlinearity is discussed.

I. INTRODUCTION

Nonradiative recombination at an impurity occurs in two steps. For example, in *p*-type material an electron in the conduction band is first captured into a bound state and then the bound electron recombines with a hole in the valence band (hole capture). During these two transitions, an energy equal to the energy gap (1.43 eV for GaAs and 2.26 eV for GaP, at room temperature) must be dissipated. Only two capture mechanisms appear to be plausible in explaining how nonradiative capture with a large energy dissipation can take place, the Auger effect^{1,2} and multiphonon emission³⁻⁸ (MPE). The energy lost by the captured carrier in Auger capture excites another nearby carrier in the crystal. The energy lost by the captured carrier in MPE capture generates lattice phonons.

A third capture mechanism that has been widely discussed is cascade capture.⁹⁻¹¹ The electron loses energy in cascade capture by dropping through a series of closely spaced levels, emitting one phonon during each transition. Lax⁹ showed that this mechanism can account for the extremely large capture cross sections exhibited by donors and acceptors at very low temperature. However cas-

cade capture cannot explain nonradiative capture into the deep levels discussed in this paper because point defects normally only have a single deep level within the forbidden gap that is far from the band edges. Neutral centers do not have excited states¹² and the hydrogenic series of excited states of a deep donor or acceptor normally lies within less than a hydrogenic donor or acceptor binding energy of the band edges (less than 50 meV in all cases). At room temperature, cascade capture of a carrier into these shallow levels will be followed by rapid emission of the carrier back into the band. Separation of the excited states and the ground state by more than an optical-phonon energy (usually many) prevents cascade capture into the ground state.

Luminescence has been an extremely powerful tool for the study of impurities in GaAs and GaP. In three instances, luminescence lifetime studies have shown definitively that nonradiative recombination was occurring by means of the Auger effect. These are the study of excitons bound to donors in GaP and Si by Nelson *et al.*,¹³ the study of excitons bound to acceptors in GaP by Dean *et al.*,¹⁴ and the study of recombination at the Zn-O center in GaP samples with varying hole concen-

trations by Jayson *et al.*¹⁵ The cross sections for these recombination processes are rather small. At a carrier concentration of $10^{18}/\text{cm}^3$ and $T=300$ K we estimate them to be approximately 10^{-19} cm^2 for the bound excitons and 10^{-18} cm^2 for the Zn-O center.¹⁶ Larger Auger cross sections are expected for deeper impurities.¹⁷ Deep impurities are also likely to have substantial relaxation of the lattice equilibrium position near the impurity after capture, which is necessary for large MPE capture cross sections. Several luminescence studies of GaAs have reported nonradiative recombination due to multiphonon emission,^{18,19} but definitive experiments which unambiguously identify recombination by MPE have not been reported.

Luminescence measurements have not been effective in studying deep nonradiative centers because such centers have broad optical emission bands and often very low luminescence efficiencies. More often the presence of deep nonradiative centers in the sample is inferred either from decreased radiative efficiency of the shallow centers,²⁰ shortening of the minority-carrier lifetime,²⁰ or from space-charge recombination in a *p-n* junction.²¹ These measurements reveal very little about the energy levels, concentrations, capture cross sections, or chemical identity of the nonradiative centers.

Recently the technique of *capacitance spectroscopy* has been developed which allows deep levels within the space-charge layer of a *p-n* junction or Schottky barrier to be directly studied.²² This technique has been refined into a precise tool for the study of deep levels in semiconductors. The various experimental methods are fully described in papers by Sah and collaborators,^{23,24} the authors and collaborators,²⁵⁻²⁸ Losee,²⁹ and Schulz.³⁰ Capacitance spectroscopy is complementary to luminescence in that it is particularly good for the study of deep levels, whether they are radiative or not, but levels less than 0.1 or 0.2 eV from the band edges may go undetected. Under favorable circumstances the concentration, the capture cross sections for electrons and holes and the energy level can be measured. Recently one of us (D.V.L.) showed that a deep level spectrum may be produced from capacitance transients during a temperature scan and all of these properties can be measured from this spectrum.²⁸ This approach is called deep level transient spectroscopy (DLTS).

Various types of capacitance spectroscopy have been employed by us to extensively survey deep levels in GaAs and GaP and in particular to measure the capture cross sections of many of these levels as a function of temperature. Both residual impurities and impurities and defects introduced by chemical doping and by radiation damage were

studied. We found that the capture cross sections of most deep levels studied in GaAs and of many deep levels studied in GaP had the magnitude and temperature dependence expected for MPE capture. This is strong evidence that nonradiative capture by MPE is commonly occurring. Most of these data were previously reported in brief publications.^{31,32} The purpose of this paper is to report these results more fully, to develop the theory of MPE and to carefully compare theory and experiment in a few cases.

Not all of the capture cross sections that we have observed in GaAs and GaP can be attributed to MPE. Some exceptions are the capture of the first electron by O in GaP,³³ and the capture of holes by Fe and Cr in GaAs.³⁴ But our work establishes that MPE capture is commonly occurring in these semiconductors and that MPE capture can give rise to large capture cross sections.

Besides causing nonradiative recombination, MPE capture can also give rise to low-temperature defect motion. Lang and Kimerling have recently shown that nonradiative recombination leads to the low-temperature annealing of radiation damage centers in GaAs,^{35,36} and in GaP.³⁷ Weeks, Tully, and Kimerling³⁸ have analyzed the GaAs experiments in terms of unimolecular reaction-rate theory and find them consistent with reasonable defect parameters. These experiments can be simply understood in terms of nonradiative recombination by MPE. This mechanism of recombination gives rise to violent, short-lived lattice vibrations localized at the defect which greatly enhance the probability of defect motion.

Nonradiative transitions by MPE are caused by crossings of free (or weakly bound) electronic states with bound electronic states. The crossings occur for sufficiently large lattice displacements. The theory of nonradiative transitions by MPE was first developed by Huang and Rhys,³ who calculated the nonradiative decay rate for the *F* center in the alkali halides. Their theory was restricted to interaction with longitudinal-optical phonons of constant frequency. This theory was extended to take into account the interactions with phonons having an arbitrary frequency distribution by Gummel and Lax,⁴ Kubo and Toyazawa,⁵ and Richayzen.⁶ All of the authors calculated transition rates between electronic states which were assumed to adiabatically follow the lattice. The calculations were simplified by making the Condon approximation, in which the relevant electronic matrix element is taken to be independent of the lattice coordinate. Kovarskii and Sinyavskii⁷ (KS) pointed out that near the crossing the adiabatic wave functions are linear combinations of the electronic states which rapidly change with lattice coordinate. These wave func-

tions cannot be represented by the Condon approximation. This was also recognized earlier by Kubo and Toyazawa⁵ who included a brief non-Condon calculation in their paper. In their non-Condon treatment, KS showed that the nonradiative rates were two to three orders of magnitude larger than rates calculated in the Condon approximation. These papers of KS are highly mathematical. Later Sinyavskii and Kovarskii⁸ (SK) published an additional paper in which they reported without derivation simple formulas to estimate the MPE capture cross sections, calculated in the semiclassical approximation. They did not make clear how the difficulties associated with the breakdown of the Condon approximation were treated in this calculation. The authors found good agreement between the calculated cross sections at high temperature and experiment for numerous attractive, neutral, and repulsive centers studied in Ge and Si. Despite their enormous success, their work has been overlooked in recent reviews and papers dealing with nonradiative capture and recombination.³⁹⁻⁴³ The commonly held view is that nonradiative recombination by MPE is of little importance.

We have not followed SK, but instead have developed our own theory of capture by MPE. We have been guided in our calculations by two simple and elegant theories of the interaction of electronic and vibrational states. The first is the theory of the line shape of phonon-broadened radiative transitions, first developed by Hwang and Rhys,³ and extended by Lax,⁴⁴ and by Kubo and Toyazawa.⁵ Nonradiative capture involves the same initial and final states as in radiative capture in which light of energy $h\nu=0$ is emitted. We find that the capture cross section can be approximately related to the line shape $f(h\nu)$ with $h\nu=0$.

The second is the theory of transitions between two states during a level crossing developed independently by Landau⁴⁵ and Zener⁴⁶ (LZ). Capture results from the crossing (or near crossing) of a free state with a bound state as the lattice vibrates. The crossing of two states may be described as sudden or adiabatic depending on the strength of the coupling between the states and the rate at which the levels cross. In a classical treatment of the lattice, LZ derived a simple formula for the transition probability valid for arbitrary coupling strength and rate of crossing. (In this treatment, the nonadiabatic operator used by KS and others in quantum-mechanical treatments of the lattice is introduced classically as the motion through the crossing point.)

We conclude this section with a brief summary of the paper. In Sec. II we discuss our experimental techniques and present data on nine capture cross sections in GaAs and four capture cross sec-

tions in GaP exhibiting the magnitude and increase with temperature expected for MPE capture. For two of the centers the cross section was found to be independent of carrier concentration, ruling out the Auger effect in these cases. In Sec. III we develop an approximate theory of MPE in which physical insight and simplicity are stressed. A detailed calculation of the capture cross section is made using a simple model in which the lattice is described by a single configuration coordinate. The capture cross section is predicted to be thermally activated

$$\sigma = \sigma_{\infty} e^{-E_{\infty}/kT}. \quad (1)$$

A detailed calculation of σ_{∞} is carried out for the case of capture by an attractive neutral impurity. The breakdown of the adiabatic approximation near the level crossing, reemission of the captured carrier immediately after capture, and nonlinear changes in the bound-state energy with lattice displacement are discussed in detail. In Sec. IV we compare theory and experiment. 12 of the 13 cross sections that we report obey Eq. (1) with σ_{∞} between 10^{-15} and 10^{-14} cm². We determine the lattice relaxation parameters for the Zn-O and O centers in GaP from optical and thermal emission data. In two cases, the observed lattice relaxation is found to be consistent with the large observed cross sections. The studies of the Zn-O and O centers also provide evidence of nonlinear changes in the bound-state energy level with the lattice displacement which greatly affect the size of the capture cross sections. In Sec. V we summarize our paper.

II. MEASUREMENT OF CARRIER CAPTURE CROSS SECTIONS

A. Techniques

The direct measurement of carrier capture cross sections by capacitance spectroscopy has been discussed previously by the authors.²⁶⁻²⁸ For completeness we will review some of the basic concepts here as well. Capacitance spectroscopy techniques use changes in the capacitance of a p - n junction or Schottky barrier as a measure of changes in the charge state of deep levels in the space-charge layer associated with the junction. With the photocapacitance method these levels are filled and emptied optically,²⁵ or filled optically and emptied with voltage pulses.²⁶ In the capacitance transient methods these deep levels in the space-charge layer are repetitively filled or emptied by voltage pulses, and the capacitance transients due to thermal emission of the trapped carriers are measured. One may study such transients at a fixed temperature^{22, 23} or by using

appropriate instrumentation obtain a spectrum of peaks corresponding to the various deep levels as a function of temperature in the DLTS method.²⁸ The capacitance change for a particular defect or impurity level is directly proportional to the concentration of that defect or impurity times a filling factor. This factor, which is between 0 and 1, is a measure of the fraction of levels filled during the voltage pulse applied to the sample. By measuring the filling factor as a function of the duration of the pulse we obtain the carrier capture rate for a particular level. The capture cross section is obtained from this rate.

For a sample with only one or perhaps two deep levels one may measure the various capture rates by looking directly at the capacitance transient or photocapacitance signal as a function of voltage pulse duration or number of voltage pulses. This was the case for the O'levels in GaP. For a more complicated spectrum one must use the DLTS method, where the capture rate is measured directly and separately for each level by fixing the temperature at the DLTS peak for that level and then measuring the peak height versus the voltage pulse duration. For these complicated spectra the temperature dependence of the cross sections is obtained by adjusting the DLTS rate window²⁸ so as to position the spectral peak associated with the level under study at the desired temperature. One then measures the peak height versus pulse duration at the various temperatures corresponding to the various spectral peak positions obtained by varying the DLTS rate window. At temperatures lower than the lowest spectral peak position obtainable (i.e., slowest practical rate window), one can obtain capture rates in simple systems by observing the capacitance changes directly.

During the observation phase of capacitance spectroscopy the deep levels are in the space-charge layer and hence subject to rather substantial electric fields which can greatly influence carrier capture and emission.²⁷ The capture phase of the pulsed bias methods, however, occurs with the observed levels in *neutral* material, due to the narrowing of the space-charge layer during the voltage pulse. Hence the capture rates and cross sections which we obtain are characteristics of the level at zero electric field.

The simplest and most accurate type of capture to measure by these techniques is the capture of majority carriers. Hence unless otherwise specified we will always be measuring majority-carrier capture via the width dependence of a majority-carrier pulse as discussed in Ref. 28. For majority-carrier capture we have

$$c_n = \sigma_n \langle v_n \rangle n, \quad n\text{-type}, \quad (2a)$$

$$c_p = \sigma_p \langle v_p \rangle p, \quad p\text{-type}, \quad (2b)$$

where with appropriate subscripts (n , electron; p , hole) c is the carrier capture rate, which is the experimentally measured quantity, σ is the carrier capture cross section, n (p) is the free-electron (hole) concentration, and $\langle v \rangle$ is the mean thermal velocity of the carrier defined by

$$\langle v \rangle \cong (\langle v^2 \rangle)^{1/2} = (3kT/m^*)^{1/2}, \quad (3)$$

where k is the Boltzmann constant, T is the absolute temperature, and m^* is the carrier effective mass. At temperatures where the donors or acceptors are completely ionized we may obtain n or p quite simply by C - V measurements on our samples. The carrier concentrations at somewhat lower temperatures can be calculated from the known donor or acceptor depth and an assumed degree of compensation (usually 0.5). In no case, however, do we measure cross sections where the carrier concentration differs from its high-temperature value by more than a factor of 2 or 3. Owing to the extremely shallow donors in n -GaAs (all ≤ 6 meV) there is no appreciable freeze out at any of our measurement temperatures and hence we use $n = N_D - N_A$ as measured by a capacitance feedback profiler⁴⁷ for σ_n in GaAs. Where both electron- and hole-capture cross sections are reported, the measurements have been made in both p - and n -type material for hole and electron capture, respectively.

The only exception to this pulsed bias method for measuring σ is the hole capture by state 2 (the two-electron state) of O in GaP.^{25,26} This is the largest cross section we have measured and hence complete filling of the level occurs even during the shortest pulse available (10 nsec). The technique used to measure this large cross section consisted of illuminating a semitransparent Schottky barrier with above band-gap light and observing the capture of photogenerated holes as they are swept through the space-charge layer. By measuring the capacitance change and photocurrent one can obtain the capture cross section.

The method and data are shown in Fig. 1. The capacitance change due to hole capture increases rapidly for photon energies greater than the energy gap and is easily distinguished from capacitance signals due to photoionization of the bound electron. The rate of hole recombination $\sigma_{p2} \langle v \rangle p$ is directly measured from the rate of change of the capacitance signal. The average field in the region of recombination, for the junction shown in Fig. 1, is about 3.3×10^4 V/cm. The drift velocity μE , assuming a mobility of 100 cm²/V sec is 0.33×10^7 cm/sec. Thus the drift velocity is much less than the thermal velocity (2×10^7 cm/sec). In this

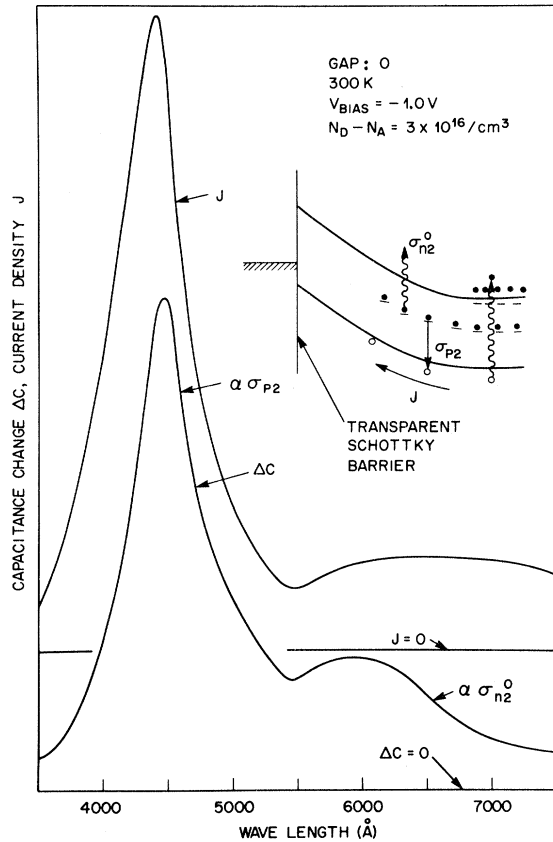


FIG. 1. Photocapacitance and photocurrent data vs the wavelength of the incident light. The signals increase for $\lambda < 5400 \text{ \AA}$ due to hole capture and then decrease for $\lambda < 4500 \text{ \AA}$ due to the decrease in light intensity.

regime $v_a \ll v_{th}$, the hole density p is related to the photocurrent J by

$$p = J / \mu e E, \quad (4)$$

where E is the junction electric field and μ is the hole drift mobility. The hole density was determined by measuring J and calculating the average value of E^{-1} . The uncertainties in the measurement of σ are largely due to uncertainties in the calculation of $\langle E^{-1} \rangle$. Additional thermal scanning experiments showed that carriers were being captured into state 2 of oxygen. The hole capture removed the bound-electron thermal emission signal of this level.

The GaAs samples used in these measurements were asymmetric step junctions (either n^+p or p^+n) grown by liquid-phase epitaxy (LPE). One GaAs sample, used to measure σ_n for an oxygen-related center, consisted of a p^+ LPE layer grown on an n -GaAs melt-grown substrate so that the observed deep levels were characteristic of the melt-grown material. The GaP samples were all grown by LPE. Hole capture was studied in pn

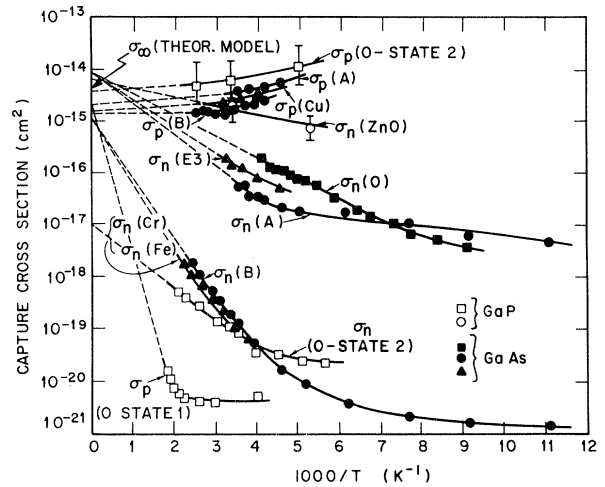


FIG. 2. Carrier-capture cross sections vs inverse temperature for various deep levels in GaAs and GaP. An n subscript denotes electron capture while a p denotes hole capture. Levels shown for GaAs are due to Cu, Fe, Cr, O, the $E3$ radiation damage defect, and two unidentified but commonly occurring levels A and B. For GaP the cross sections are associated with the Zn-O center and the two states of the oxygen center. The dashed lines show the temperature dependence of the cross sections extrapolated to $T = \infty$. The value of σ_∞ predicted by the theoretical model is indicated on the ordinate.

junctions doped with Zn and O on the p side. Electron capture was measured in Schottky barriers on n -type material doped with oxygen. The carrier concentrations of the various samples ranged from the mid- $10^{15}/\text{cm}^3$ range to the mid- $10^{17}/\text{cm}^3$ range. No dependence of cross section on carrier concentration was observed.

B. Carrier capture data

Figure 2 shows the temperature dependence of 13 capture cross sections in GaAs and GaP measured by the above techniques. Note the large vertical scale (eight orders of magnitude). One can immediately see a general trend. Many of the levels have cross sections which increase exponentially with temperature. In addition we find increasingly larger slopes for correspondingly smaller cross sections. The activation energies obtained at the highest temperature for some of the small cross sections are rather large, from 80 to 560 meV. This is a significant fraction of the depths of the levels. The 13 cross sections which we discuss here as showing evidence of MPE have been selected from many others which we have observed. Some levels do not show evidence for MPE, others do exhibit the characteristic exponential MPE behavior but have been omitted be-

cause their origin is not well defined. The data we present is either on levels of known chemical origin or levels that can be reliably reproduced under controlled conditions.

Three of the four cross sections shown in Fig. 2 for GaP are for the O center which has two states (state 1 and state 2) which deeply binds one and two electrons, respectively, and whose optical properties are well known.^{25,26} We show the hole-capture cross section for the one-electron state and the hole- and electron-capture cross section for the two-electron state. The electron-capture cross section for the one-electron state is omitted since it shows no evidence of MPE capture. Also shown is the electron-capture cross section for the Zn-O center in GaP as reported in the literature.^{27,48} In Sec. IV the agreement between theory and experiment for these four cross sections will be discussed in detail.

The nine GaAs cross sections shown are for seven different levels. Those labeled *A* and *B* are two unidentified levels at $E_v + 0.40$ eV and $E_v + 0.71$ eV which are the only deep levels present in undoped LPE GaAs; they occur in nearly all samples at a concentration of about $10^{15}/\text{cm}^3$ for each. The observation of these levels in many different samples indicates that they are due either to native defects or to some ubiquitous chemical impurity. DLTS measurements on intentionally doped GaAs show that level *A* and *B* are not, however, due to Cu, Fe, Mn, or Cr since these all have distinctly different spectra.³⁴

The level *E3* at $E_c - 0.31$ eV due to 1-MeV electron radiation damage is one of the defects observed by Lang and Kimerling^{35,36} which exhibits recombination enhanced diffusion, a process closely related to MPE capture. This is clearly some sort of native defect.

The electron-capture cross section labeled $\sigma_n(0)$ is for a level in melt-grown *n*-GaAs which is most likely due to an oxygen-related center. The capacitance transient due to this level has been observed by numerous workers in melt-grown GaAs,^{22,49-51} and vapor-phase epitaxial (VPE) GaAs,⁵²⁻⁵⁵ both with and without intentional oxygen doping. It has not, however, been observed in LPE GaAs.³⁴ It has been associated with the *i* layer that occasionally occurs between the GaAs substrate and a VPE layer.⁵² The activation energy for emission of an electron from this level is 0.89 eV and thus it would not at first sight appear to be oxygen which is reported to be at $E_c - 0.75$ eV by Hall measurements.⁵⁶ However, when the electron-capture cross section exhibits a strong temperature dependence as in Fig. 2, one must correct the observed activation energy for emission to obtain the true energy depth of the level. The emis-

sion rate e is related to the level depth ΔE by detailed balance as

$$e = \sigma \langle v \rangle N e^{-\Delta E/kT} / g, \quad (5)$$

where N is the density of states in the band to which the carrier is emitted and g is the degeneracy of the level. If the preexponential factor were independent of temperature, then the slope of $\ln e$ vs $(kT)^{-1}$ (which we call ΔE_{meas} , the activation energy for carrier emission) would be nearly equal to the true level depth ΔE . But if $\sigma = \sigma_\infty e^{-E_\infty/kT}$, as is the case in Fig. 2 at higher temperatures, then $\Delta E_{\text{meas}} = \Delta E + E_\infty$ in this temperature range. Thus the activation energy for carrier capture must be subtracted from the activation energy for carrier emission to obtain the true level depth. An additional small correction arises from the fact that $\langle v \rangle N$ is proportional to T^2 . When the 80-meV capture activation energy and T^2 correction ($\approx 2kT$) are subtracted from 0.89 eV, we obtain a level depth of $E_c - 0.75$ eV which is the level of the oxygen donor obtained by Hall analysis of semi-insulating oxygen-doped GaAs.⁵⁶ All energy levels used in this paper have been corrected for T^2 and E_∞ in this same manner.

Finally, three levels due to transition element impurities (Cr, Fe, and Cu) in GaAs are shown in Fig. 2. These centers have been produced by doping the LPE layer with the impurity during growth.³⁴ The energy levels obtained by DLTS with the corrections outlined above agree with the levels of these impurities reported in the literature,⁵⁶ namely ($E_v + 0.52$ eV) for Fe, ($E_v + 0.79$ eV) for Cr, and ($E_v + 0.44$ eV) for Cu.³⁴ These levels are known to be acceptors from Hall data. Therefore σ_n corresponds to capture by a neutral center while σ_p corresponds to capture by an attractive Coulomb center. As shown in Fig. 2, the electron-capture cross sections for the Cr and Fe centers and that for level *B* are practically identical over the temperature range of measurement (285–435 K). This is rather remarkable in view of the fact that these three centers have quite different energy levels and DLTS spectra, ranging from 0.52 to 0.79 eV above the valence band. The hole-capture cross section for Cu is also shown in Fig. 2. This cross section has very little temperature dependence and is very similar to the hole-capture cross sections of levels *A* and *B* in GaAs and O state 2 in GaP. The hole-capture cross sections for Fe and Cr have been measured³⁴ but not included in Fig. 2 since they do not show evidence of MPE capture.

C. Search for Auger effect

We have taken the strongly temperature-dependent cross sections shown in Fig. 2 as evidence

for carrier capture by the MPE mechanism. Band-to-band Auger processes can be thermally activated due to the necessity to conserve momentum among the free carriers involved. Such exponential behavior with large activation energies is thought not to be a property of the free-to-bound Auger effect since the deep level can provide the necessary momentum for the second carrier.^{2,17} In addition we have direct evidence that at least three of the cross sections are not due to the Auger effect. Two of the cases involve majority-carrier electron capture at a deep unoccupied level. In this case the Auger capture is proportional to the square of the carrier concentration.

The data are for two single-particle centers in GaAs: level *B* ($E_v + 0.71$ eV) and Cr ($E_v + 0.78$ eV). In order to conclusively rule out the Auger effect in these cases we have studied the electron-capture cross section over a wide range of electron concentrations. Figure 3 shows the cross-section data for level *B* in GaAs measured in seven different samples with net donor concentrations varying by a factor of 23 from $4.2 \times 10^{15}/\text{cm}^3$ to $9.5 \times 10^{16}/\text{cm}^3$. There is no dependence on carrier concen-

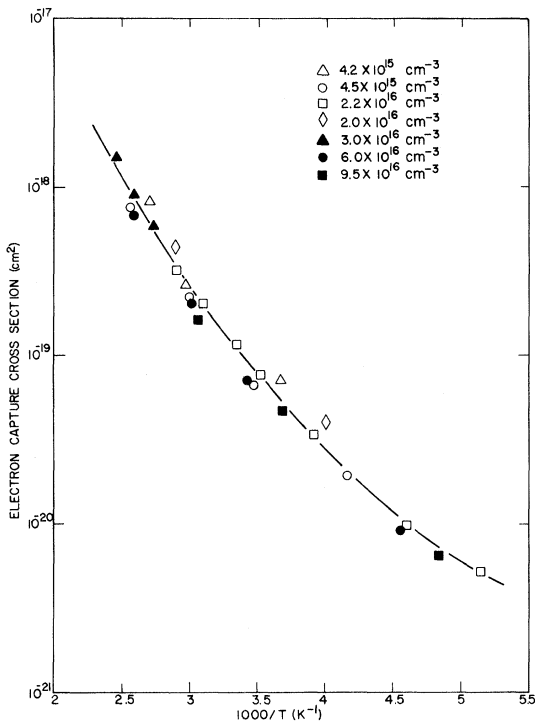


FIG. 3. Electron-capture cross section of level *B* in *n*-GaAs [$\sigma_n(B)$] vs inverse temperature for seven samples of various electron concentration. The concentration of electrons varies by a factor of 23 and is shown next to the sample number in units of cm^{-3} . Note that the cross section is independent of carrier concentration within experimental scatter.

tration within the $\pm 25\%$ scatter of the experimental points. This scatter is due to the uncertainty in the measured net donor concentrations from sample to sample. If the Auger effect were the cause of this large temperature dependence, $E_\infty = 0.25$ eV at 400 K, we would have observed a variation of a factor of 23 in cross section. The σ_n for Cr, shown in Fig. 2, behaves similarly.

The third case where the Auger effect can be ruled out is the hole-capture cross section of the second electron on the oxygen center in GaP. In this case the Auger effect is definitely not possible since the first electron is observed to remain trapped even after the second electron has recombined with a hole.²⁶

III. THEORY OF CAPTURE BY MULTIPHONON EMISSION

A. Overview

Nonradiative capture takes place because the energy of a deep level depends on the positions of the atoms comprising the defect and its neighbors, that is, the lattice. As the lattice vibrates the level moves up and down in the energy gap. The diagram in Fig. 4 illustrates a simple model of the electron lattice interaction in which for simplicity the lattice is represented by a single co-

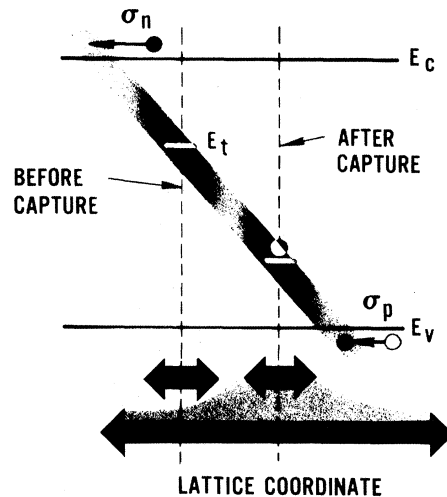


FIG. 4. Diagram illustrating how nonradiative capture of an electron takes place. The equilibrium positions of the lattice coordinate and the energy level, before and after capture, are indicated by the dashed lines. The shaded regions within the energy gap indicate how the energy of the level changes as the lattice vibrates. The smaller arrows represent the amplitudes of the thermal vibrations, before and after capture of an electron. The large arrow represents the amplitude of the lattice vibrations about the new equilibrium position, immediately after capture.

ordinate. Consider the nonradiative capture of an electron illustrated in Fig. 4. Prior to capture, the equilibrium position of the level is in the upper half of the gap. For sufficiently large vibrations the level can cross into the conduction band and capture an electron. After capture of the electron the lattice near the defect relaxes in such a way as to lower the equilibrium position of the level in the energy gap.

It is clear from the figure that immediately after capture of the electron the lattice is displaced far from the new equilibrium position and there will be a violent lattice vibration at the defect. The vibration will rapidly damp down to the amplitude of thermal vibrations after a small number of vibrational periods. During the damping, the localized energy propagates away from the defect as lattice phonons. This justifies calling this process nonradiative capture by multiphonon emission (MPE). We assume that the large amplitude vibrations occurring at the defect during MPE capture are the cause of the recombination induced defect motion observed by Lang and Kimerling.³⁵⁻³⁷

Roughly speaking, the capture cross section is proportional to the product of three probabilities

$$\sigma \propto P_{\text{vib}} P_{\text{ct}} P_{\text{tt}}.$$

P_{vib} is the probability that sufficiently strong lattice vibrations will occur so that the energy level of bound state $|t\rangle$ will twice cross (or nearly cross) an occupied conduction-band state $|c\rangle$ during each vibrational period. P_{ct} is the probability that during the double crossing a capture transition occurs. P_{tt} is the probability that after capture, the electron will not be reemitted into another conduction band level, during subsequent level crossings which occur before level t leaves the conduction band.

At high temperatures $P_{\text{vib}} \approx e^{-E_B/kT}$, where E_B is the lattice energy necessary for a level crossing when the bound state is unoccupied [see Fig. 5(b)]. P_{vib} determines the thermally activated behavior of the MPE capture cross sections. The variation of E_B for different centers produces most of the large variation in the magnitudes of the capture cross sections observed for different centers at room temperature and lower temperatures.

In Secs. III B–III E we carry out a detailed calculation of the capture cross section for the capture of an electron by a neutral impurity using an extremely simple model. We describe the lattice by a single configuration coordinate Q and coupling of the impurity to the lattice by allowing the well depth to change linearly with Q . We also assume for simplicity that the energy of the bound state changes linearly with Q . It is convenient to write the capture cross section as

$$\sigma = \sigma_c P_{\text{tt}}, \quad (6)$$

where σ_c is the cross section for initial capture and P_{tt} is the probability that the electron is not reemitted. We calculate σ_c treating the lattice as quantized vibrations in Sec. III B and treating the lattice as a classical variable in Sec. III C. The classical calculation is only valid at high temperatures, but it is useful in that it provides insight into the nature of the capture transition and the breakdown of the adiabatic approximation near the level crossing. Both calculations agree in the high-temperature limit. Cross section σ_c depends on an electronic matrix element. We evaluate this matrix element under the assumption that both the bound state and the free-carrier state wave functions can be described in the effective-mass approximation with both states associated with the same band. We make a rough estimate of P_{tt} in Sec. III E. Finally in Sec. III F we will briefly consider other effects not treated in this simple model including nonlinear changes of the energy of the bound state versus Q , charged centers, recombination after capture, and capture when the free-carrier state and the bound state have different symmetries.

B. Calculation of σ_c treating the lattice as quantized

1. Model

Let us consider capture of an electron by a neutral impurity. The impurity and its nearest neighbors form a potential well which can bind an electron. For simplicity, we will take the potential well to be spherical with a radius b equal to the nearest-neighbor distance and a depth V_0 . Parameters b and V_0 will not enter into our final formulas. The depth of the potential well is a sensitive function of the positions of the impurity and the neighboring atoms. To model this behavior we will describe the vibrations of these atoms by a single lattice coordinate Q .

The Hamiltonian for this system is

$$\begin{aligned} H &= H_E + H_{EL} + H_L \\ &= [p^2/2m^* + V(r)] \\ &\quad + BQV(r) + (P^2/2M + \frac{1}{2}M\omega^2Q^2). \end{aligned} \quad (7)$$

H_E is the electronic Hamiltonian with $Q=0$, H_{EL} describes the change in the potential-well depth by a lattice displacement Q , and H_L is the Hamiltonian of a harmonic oscillator vibrating about $Q=0$. Let

$$|c\rangle = \varphi_c(\vec{r}), \quad |t\rangle = \varphi_t(\vec{r}), \quad |v\rangle = \varphi_v(\vec{r})$$

be the eigenfunctions of H_E for a free state at the bottom of the conduction band, a trapped electron,

and a free state at the top of the valence band, respectively. (These wave functions are independent of Q . They correspond to the adiabatic states at $Q=0$. Later we will consider the changes in the wave functions with Q .) Let us first plot the energies of these states regarding Q as a parameter. The electronic energies of the states $i = c, v, t$ are

$$E_i(Q) = \langle i | p^2/2m^* + V(r) + BQV(r) | i \rangle. \quad (8)$$

These energies are shown in Fig. 5(a). For a free state $|c\rangle$ or $|v\rangle$, the energy is independent of Q since the probability of the electron being in the potential well is negligible and therefore $BQ\langle c | V | c \rangle \approx 0$, etc. On the other hand, the matrix element $BQ\langle t | V(r) | t \rangle$ may be large and this term causes

the bound state to cross into the conduction band at $Q = Q_c$ and into the valence band at $Q = Q_v$.

For the electron in state $i = c, t, v$, the potential well for the lattice $U_i(Q)$ is

$$U_i(Q) = E_i(Q) + \frac{1}{2}M\omega^2Q^2. \quad (9)$$

These wells are plotted in Fig. 5(b). Note that the lattice equilibrium position is at $Q=0$ regardless of whether the electron is in the conduction band or valence band. The harmonic-oscillator states of the wells are also shown in Fig. 5(b). We will denote these states as $|n_c\rangle$, $|n_t\rangle$, and $|n_v\rangle$. The complete wave functions of the electron and the lattice are approximately given by $|c\rangle|n_c\rangle$, etc. These are not exact eigenstates because the perturbation $BQV(r)$ couples states $|t\rangle$ with $|c\rangle$ and $|v\rangle$. Of course, it is just this coupling that causes capture of a free electron into the bound state. These wave functions represent an extreme approximation in which the electronic states are assumed not to change as the lattice vibrates.

2. Dependence of the electronic wave functions on Q

A better approximation away from level crossings is the adiabatic approximation. In this approximation, the electronic states are assumed to have the same wave functions at each position Q that they would have if Q were fixed at this position. Consider the capture of an electron from the conduction band. For a large energy separation of states $|c\rangle$ and $|t\rangle$, the electronic states will adiabatically follow the lattice. But as the lattice approaches the crossing point ($Q = Q_c$ in Fig. 5), the adiabatic approximation requires that the electron wave function change completely from a free state to a bound state during the small fraction of a vibrational period. This requirement cannot possibly be satisfied because the coupling between the free state $|c\rangle$ and bound state $|t\rangle$ is infinitesimal. Consequently the adiabatic approximation breaks down near the crossing.

It will be shown in Sec. III C2 that the breakdown occurs at approximately $\epsilon_1 \approx 0.06$ eV away from the level crossing and transitions begin at this point. It will also be shown that the total probability of a transition at each crossing is infinitesimal and readily calculated using first-order time-dependent perturbation theory.

In this section we will assume this to be the case without further justification. Let us assume that the adiabatic approximation begins to significantly break down at $Q = Q_1$, where the bound state is an energy ϵ_1 below the crossing. Referring to Fig. 5(a) let $\epsilon(Q) = E_c - E_t(Q)$. To incorporate both the adiabatic approximation and its breakdown into the calculation of σ_c we will take the electronic

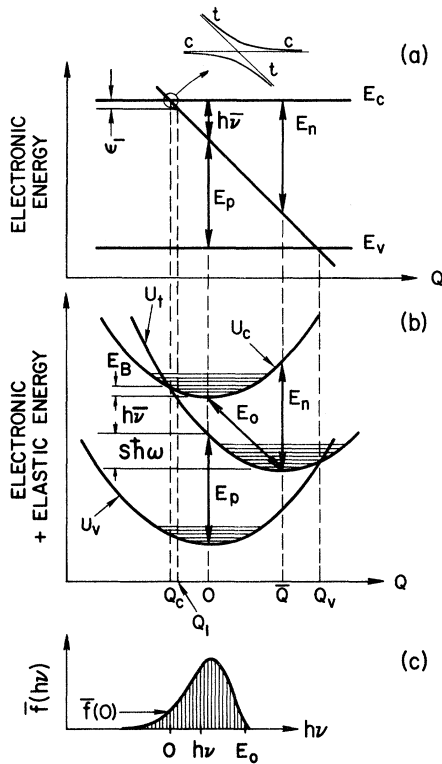


FIG. 5. (a) Electronic energies vs lattice coordinate Q . The adiabatic approximation is assumed to break down at Q_1 where the level is $\epsilon_1 \approx 0.06$ eV below the conduction band. The insert shows the adiabatic and non-adiabatic states in the crossing region. (b) The configuration coordinate diagram - electronic + elastic energies vs Q . The thermal barrier height E_B , the increase in binding energy due to lattice relaxation $S\hbar\omega$, and the total binding energy E_0 are indicated. The optical excitation thresholds at lattice equilibrium before relaxation E_p and after relaxation E_n are also indicated. (c) Line shape for radiative capture. The vertical lines indicated $f(h\nu)$, which is a series of delta functions. The smooth curve $\bar{f}(h\nu)$ reflects the integrated strength of these δ functions.

wave functions to be the adiabatic wave functions $|c\rangle = u_c(\mathbf{r}, Q)$, $|t\rangle = u_t(\mathbf{r}, Q)$, etc., for values of Q such that $|\epsilon| > \epsilon_1$. At $Q = Q_1$, $\epsilon = \epsilon_1$ we will change to the sudden approximation. In the crossing region $|\epsilon| < \epsilon_1$ we will assume $|t\rangle$ and $|c\rangle$ no longer change with Q and have the values of adiabatic states at $Q = Q_1$. That is $|c\rangle = u_c(\mathbf{r}, Q_1)$, $|t\rangle = u_t(\mathbf{r}, Q_1)$, for $|\epsilon| < \epsilon_1$. The justification of this approximation is given in Sec. III C 2.

3. Relation between σ_c and the line shape for radiative capture

The transition rate for capture of an electron is given by

$$w = \frac{2\pi}{\hbar} \text{ave}_{n_c} \sum_{n_t} |\langle n_t | \mathcal{H} | c n_c \rangle|^2 \delta(\mathcal{E}_c - \mathcal{E}_t), \quad (10)$$

where $\mathcal{E}_c = n_c \hbar \omega$ and $\mathcal{E}_t = n_t \hbar \omega - E_0$. Only the off-diagonal parts of \mathcal{H} contribute to the matrix element. The vibrational wave functions $|n_t\rangle$ and $|n_c\rangle$ are highly oscillatory and overlap strongly only in the region $|Q - Q_c| < Q_1$. In this region the electronic states $|c\rangle$ and $|t\rangle$ are independent of Q . They are the assumed eigenstates of $p^2/2m^* + V(Q)$ with $Q = Q_1$. We can make use of this fact by writing $V(\mathbf{r}, Q) = V(\mathbf{r}, Q_1) + \Delta V(\mathbf{r}, Q) = V_1 + \Delta V$:

$$\begin{aligned} \langle t | \mathcal{H}_E + \mathcal{H}_{EL} + \mathcal{H}_L | c \rangle &= \langle t | p^2/2m^* + V_1 | c \rangle \\ &+ \langle t | \Delta V | c \rangle + \langle t | c \rangle \mathcal{H}_L \\ &= \langle t | \Delta V | c \rangle. \end{aligned} \quad (11)$$

The first and third terms in Eq. (11) are zero because of the orthogonality of $|c\rangle$ and $|t\rangle$ and because $p^2/2m^* + V_1$ is diagonal in these states. Because ΔV is slowly varying, we will take it as constant and equal to its value at the crossing point $Q = Q_c$:

$$\Delta V \approx B(Q_c - Q_1)V. \quad (12)$$

With this simplification Eq. (10) becomes

$$w = \frac{2\pi}{\hbar} |\langle t | \Delta V | c \rangle|^2 \left(\text{ave}_{n_c} \sum_{n_t} |\langle n_t | n_c \rangle|^2 \delta(\mathcal{E}_c - \mathcal{E}_t) \right). \quad (13)$$

The complex term in the large parentheses can be related to the line shape for radiative capture. The line shape $f(h\nu)$ is a well-known function of $\hbar\omega$, E_B , and kT .

The rate of radiative capture, at which light of energy $h\nu$ is emitted, is

$$\frac{dw^{\text{rad}}}{d(h\nu)} = \frac{2\pi}{\hbar} \text{ave}_{n_c} \sum_{n_t} |\langle u_t n_t | H_{\text{rad}}(\mathbf{r}) | u_c n_c \rangle|^2 \times \delta(\mathcal{E}_c - \mathcal{E}_t - h\nu) \rho_{\text{rad}}. \quad (14)$$

In a radiative transition, the normal approximation

(the Condon approximation) is to estimate the electronic states by their values at $Q = 0$, that is, by φ_c and φ_t . Then

$$\begin{aligned} \frac{dw^{\text{rad}}}{d(h\nu)} &= \frac{2\pi}{\hbar} \rho_{\text{rad}} |\langle \varphi_t | H_{\text{rad}} | \varphi_c \rangle|^2 \\ &\times \text{ave}_{n_c} \sum_{n_t} |\langle n_c | n_t \rangle|^2 \delta(\mathcal{E}_c - \mathcal{E}_t - h\nu). \end{aligned} \quad (15)$$

We define the normalized line shape $f(h\nu)$ as

$$f(h\nu) = \text{ave}_{n_c} \sum_{n_t} |\langle n_t | n_c \rangle|^2 \delta(\mathcal{E}_c - \mathcal{E}_t - h\nu). \quad (16)$$

Noting that $\rho_{\text{rad}} |\langle t | H_{\text{rad}} | c \rangle|^2 \sim (h\nu)^3$,⁵⁷ we find

$$\frac{dw^{\text{rad}}}{d(h\nu)} \sim (h\nu)^3 f(h\nu). \quad (17)$$

$f(h\nu)$ is sketched in Fig. 5(c).

The nonradiative transition rate Eq. (13) is clearly proportional to $f(0)$. The capture cross section σ_c is related to the nonradiative transition rate w by

$$\sigma_c = (\Omega/\langle v \rangle) w, \quad (18)$$

where Ω is the volume of the crystal and $\langle v \rangle$ is the thermal velocity of the free carrier. Substituting Eqs. (13) and (16) into Eq. (18), we have

$$\sigma_c = A f(0), \quad (19)$$

where

$$A = (2\pi\Omega/\hbar\langle v \rangle) |\langle c | \Delta V | t \rangle|^2. \quad (20)$$

Other approximate derivations relating the nonradiative transition rate to $f(0)$ have been given by Kubo and Toyazawa⁵ and by Engelman and Jortner.⁵⁹ Equation (19) follows from the fact that essentially the same initial or final vibrational states enter into the nonradiative transition as enter into a radiative capture transition in which light of zero energy is emitted. For $h\nu = 0$, the radiative rate is zero due to the $(h\nu)^3$ factor in Eq. (17), however $f(h\nu)$ may be nonzero. In both the radiative and nonradiative transitions the electronic matrix element can be approximated as constant independent of Q . In the radiative transition this matrix element is evaluated using the adiabatic wave functions at $Q = 0$. In the nonradiative transition considered here, we evaluate it using the adiabatic wave functions at $Q = Q_1$.

We shall show that the coefficient A does not depend sensitively on the properties of the impurity or the host crystal, and that the large variations in the magnitudes of capture cross sections and the temperature dependence of these cross sections are determined almost entirely by $f(0)$; $f(0)$ is determined by the lattice relaxation prop-

erties of the center. These properties are very difficult to calculate from first principles. Instead of making this calculation we shall compare theory and experiment in this paper by determining $f(0)$ experimentally by means of optical and thermal emission measurements.

4. Temperature dependence of $f(0)$ and σ_c

The line shape $f(h\nu)$ was calculated by Huang and Rhys.³ It depends on three parameters E_0 , $\hbar\omega$, and S defined in Fig. 5(b):

$$f(h\nu) = \sum_{p=-\infty}^{\infty} \delta(E_0 - p\hbar\omega - h\nu) W_p, \quad (21)$$

$$W_p = \exp[-(2n+1)S][(\bar{n}+1)/\bar{n}]^{p/2} \times I_p(2S[(\bar{n}+1)\bar{n}]^{1/2}), \quad (22)$$

where I_p is the modified Bessel function of order p and

$$\bar{n} = [\exp(\hbar\omega/kT) - 1]^{-1}. \quad (23)$$

The line shape is sketched in Fig. 5(c). It consists of a series of δ functions. In reality mode Q will be strongly coupled to the rest of the lattice so that the vibrations of Q will be strongly damped. This will cause the levels n_c and n_t to be lifetime broadened. Also, the center will be coupled to a number of different lattice modes with different frequencies. These effects cause the series of sharp lines in $f(h\nu)$ to be broadened into a smoothed line shape which we call $\bar{f}(h\nu)$. $\bar{f}(h\nu)$ is sketched in Fig. 5(c):

$$\bar{f}(h\nu) = W_p/\hbar\omega. \quad (24)$$

The moments of $f(h\nu)$ have been calculated by Lax.³⁹ The first two moments of the line shape are

$$\langle h\nu \rangle = h\bar{\nu} = E_0 - S\hbar\omega \quad (25)$$

and

$$\langle (h\nu - h\bar{\nu})^2 \rangle = \langle E^2 \rangle = S(\hbar\omega)^2(2\bar{n} + 1). \quad (26)$$

These moment formulas are useful in determining S and $\hbar\omega$ from luminescence data. In the limit of large S , $\bar{f}(h\nu)$ approaches a Gaussian line shape predicted by the Franck-Condon principle^{44, 58}

$$\bar{f}(h\nu) \rightarrow (2\pi\langle E^2 \rangle)^{-1/2} \exp[-(h\nu - h\bar{\nu})^2/2\langle E^2 \rangle]. \quad (27)$$

At high temperatures $\bar{n} \rightarrow kT/\hbar\omega$, $\langle E^2 \rangle \rightarrow 2\hbar\omega kTS$, and

$$\sigma_c = A\bar{f}(0) \rightarrow A(4\pi\hbar\omega kTS)^{-1/2} \exp(-E_B/kT) \\ = \left(\frac{4\pi E_B}{kT}\right)^{1/2} \frac{\Omega |\langle t | \Delta V | c \rangle|^2}{\hbar \langle v \rangle \hbar \bar{\nu}} e^{-E_B/kT}, \quad (28)$$

where

$$E_B = (h\bar{\nu})^2/4\hbar\omega S = (E_0 - \hbar\omega S)^2/4\hbar\omega S \quad (29)$$

A similar derivation of Eqs. (28) and (29) has been given by Engelman and Jortner.⁵⁹ Thus at high temperatures the cross sections are expected to increase exponentially with temperature with activation energy E_B . E_B is identified in Fig. 5(b).

The optical line-shape formula calculated by Hwang and Rhys is exactly the same whether the center is coupled to a single lattice coordinate or any number of lattice coordinates with the same frequency.⁶⁰ Consequently a very good physical understanding of phonon-broadened optical line shapes is gained by considering only a single lattice coordinate. By analogy, we expect that our analysis, based on a single coordinate model, is a reasonable approximation to the real problem.

The broadening of the line shape by the coupling of Q to the rest of the lattice has two important consequences. First, we do not have to worry about whether the initial level n_c and final level n_t are lined up. The broadening of these levels will result in the same transition rate regardless of the alignment of these levels. Second, after the transition, the vibrations about the new equilibrium position will be rapidly damped. The large vibrational energy, which is initially localized at the center, will propagate away from the center in the form of lattice phonons.

C. Calculation of σ_c with a classical lattice

In this section we will again calculate the capture cross section σ_c , neglecting reemission of the electron after capture. We assume the lattice vibrates sinusoidally about $Q=0$:

$$Q = Q_M \cos \omega t. \quad (30)$$

The level separation of the initial carrier state c and the bound electron state t is

$$\epsilon(Q) = E_c - E_t = h\bar{\nu} - E_M \cos(\omega t). \quad (31)$$

We can expand the wave function Φ in terms of eigenstates of $\mathcal{H} = p^2/2m^* + V(Q)$ at $Q=Q_1$, where Q_1 is sufficiently far from the crossings that the adiabatic approximation is valid. [We will show that the adiabatic approximation holds up to an energy separation $\epsilon_1 \approx 0.06$ eV of the level crossing. Consequently Q_1 is drawn close to the crossing in Fig. 5(a).]

$$\Phi = \sum_c a_c(t) \exp\left(-i \frac{E_c}{\hbar} t\right) |c\rangle \\ + a_t(t) \exp\left(-i \int \frac{E_t}{\hbar} dt\right) |t\rangle. \quad (32)$$

The Schrödinger equation

$$i\hbar\dot{\Phi} = [p^2/2m^* + V_1 + \Delta V(Q)]\Phi \quad (33)$$

leads to the coupled equations

$$\dot{a}_c = \frac{\langle c | \Delta V | t \rangle}{i\hbar} \exp\left(-i \int \frac{(E_t - E_c)}{\hbar} dt\right) a_t, \quad (34a)$$

$$\dot{a}_t = \sum_c \frac{\langle t | \Delta V | c \rangle}{i\hbar} \exp\left(i \int \frac{(E_t - E_c)}{\hbar} dt\right) a_c. \quad (34b)$$

Assume initially at time $t = -t_1$, $Q = Q_1$, and $E_c - E_t = \epsilon_1$, that only state c is occupied:

$$a_c(-t_1) = 1,$$

$$a_{c'}(-t_1) = a_t(-t_1) = 0, \quad c' \neq c.$$

As t increases from $-t_1$ to t_1 , the lattice will move sinusoidally to negative values of Q and back to Q_1 , causing a double crossing or a near crossing of the energy levels. The probability of a capture transition is $|a_t(t_1)|^2$.

In solving for a_t we must keep in mind that $\langle t | \Delta V | c \rangle$ is infinitesimal, since it is proportional to $\Omega^{-1/2}$ (where Ω is the volume of the crystal), due to the normalization of $|c\rangle$. Thus a_c can only change by an infinitesimal amount from unity during the transition time and we are justified in setting $a_c = 1$.

To develop an intuitive understanding of how $a_t(t)$ changes during a crossing let us neglect the coupling of the bound state to other states $c' \neq c$ and solve Eq. (34b) for $a_t(t)$ as the lattice passes through the Q_c during a large amplitude vibration. Let us approximate matrix element $\langle c | \Delta V(Q) | t \rangle$ to be constant independent of Q and equal to its value at $Q = Q_c$. Then the equation for $a_t(t)$ reduces to

$$a_t(t) = \frac{\langle t | \Delta V | c \rangle}{i\hbar} \int_{-t_1}^t e^{i\varphi(t)} dt, \quad (35a)$$

$$\varphi(t) = \int^t \left(\frac{E_t - E_c}{\hbar} \right) dt. \quad (35b)$$

1. Calculation of σ_c assuming the levels cross at a uniform rate

We will assume that $E_t - E_c$ changes linearly with time near the level crossing and write the phase factor in Eq. (35b) as

$$\varphi(t) = \dot{E}_t \frac{(t - t_c)^2}{2\hbar} = \frac{\pi}{2} \frac{(E_t - E_c)^2}{(\Delta E)^2}, \quad (36)$$

where ΔE is defined by this equation. For sinusoidal motion, the rate of level crossing \dot{E}_t is related to E_M and $\hbar\bar{\nu}$ by

$$|\dot{E}_t|_{E_t = E_c} = \omega(E_M^2 - \hbar^2\bar{\nu}^2)^{1/2} \quad (37)$$

and

$$\Delta E = (\pi\hbar|\dot{E}_t|)^{1/2} = (\pi\hbar\omega)^{1/2}(E_M^2 - \hbar^2\bar{\nu}^2)^{1/4}. \quad (38)$$

This is exactly the problem solved by LZ, except in our case the problem is greatly simplified because $\langle t | \Delta V | c \rangle$ is infinitesimal. The integration of Eq. (35a) is

$$a_t = \frac{\langle t | \Delta V | c \rangle}{i\hbar} \pi \int_{E_{t_1}}^{E_t} dE_t \exp\left(i \frac{\pi}{2} \frac{(E_t - E_c)^2}{(\Delta E)^2}\right) \\ = \langle t | \Delta V | c \rangle / i \Delta E \pi [C(x) + iS(x)]_{x(E_{t_1})}^{x(E_t)}, \quad (39)$$

where $x = (E_t - E_c) / \Delta E$, and $C(x)$ and $S(x)$ are Fresnel integrals defined by

$$C(x) = \int_0^x \cos\left(\frac{\pi x^2}{2}\right) dx = -C(-x), \quad (40)$$

$$S(x) = \int_0^x \sin\left(\frac{\pi x^2}{2}\right) dx = -S(-x).$$

Figure 6 shows a plot of $|a_t(x)|^2$ computed from Eq. (39), with $x(E_{t_1}) = -\infty$. The increase of $|a_t|^2$

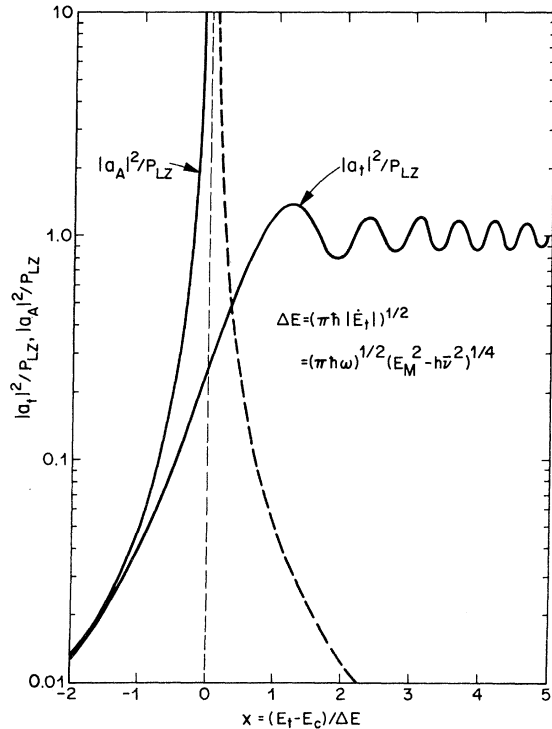


FIG. 6. Squared amplitude of the bound state $|a_t|^2$ divided by the single pass transition probability of the Landau-Zener theory P_{LZ} as a function of the level separation $E_t - E_c$. $|a_A|^2$ is the calculation of $|a_t|^2$ in the adiabatic approximation. As the crossing is approached $|a_A|^2 \rightarrow 1$ and $|a_A|^2/P_{LZ} \rightarrow \infty$. The dashed curve shows the decrease in $|a_A|^2/P_{LZ}$ above the crossing predicted by Eq. (50). In a more exact treatment of the adiabatic approximation a_A would remain equal to unity above the crossing.

take place primarily in the range where E_t is within an energy $\frac{1}{2}\Delta E$ of the crossing. The increase in $|a_t|^2$ due to the crossing is P_{LZ} , where

$$P_{LZ} = \frac{2\pi}{\hbar} \frac{|\langle c | \Delta V | t \rangle|^2}{|\dot{E}_t|} = \frac{2\pi}{\hbar\omega} \frac{|\langle c | \Delta V | t \rangle|^2}{(E_M^2 - \hbar^2\bar{\nu}^2)^{1/2}}. \quad (41)$$

P_{LZ} is exactly the single crossing transition probability predicted by the LZ theory when $P_{LZ} \ll 1$. (In our case P_{LZ} is infinitesimal.)

Let us calculate the thermal average of the single crossing transition probability P , which we assume to be equal to P_{LZ} for $E_M \geq \hbar\bar{\nu}$ and zero for $E_M < \hbar\bar{\nu}$. A more rigorous thermal average will be carried out in Sec. III C3. We can relate $E_M^2 - \hbar^2\bar{\nu}^2$ to the energy of lattice vibrations by referring to Fig. 5(a):

$$E_M^2/\hbar^2\bar{\nu}^2 + Q_M^2/Q_C^2 = E_Q/E_B, \quad (42)$$

where Q_M is the maximum amplitude of the lattice vibration of energy E_Q , and Q_C and E_B denote these parameters for a vibration which has a turning point at the level crossing. Using Eq. (42), Eq. (41) becomes

$$P = P_{LZ} = \frac{2\pi}{\hbar\omega} \frac{|\langle c | \Delta V | t \rangle|^2 (E_B)^{1/2}}{\hbar\bar{\nu}(E_Q - E_B)^{1/2}}, \quad E_Q \geq E_B, \quad (43)$$

$$P = 0, \quad E_Q < E_B.$$

The thermal average of P reduces to calculating the thermal average of $(E_Q - E_B)^{-1/2}$ for $E_Q > E_B$. Assuming the lattice energies obey a Boltzmann distribution, which is valid for $kT \gtrsim \hbar\omega$, we have

$$\langle (E_Q - E_B)^{-1/2} \rangle = \int_{E_B}^{\infty} dE_Q e^{-E_Q/kT} (E_Q - E_B)^{-1/2} \Big/ \int_0^{\infty} dE_Q e^{-E_Q/kT} = e^{-E_B/kT} (\pi/kT)^{1/2} \quad (44)$$

and

$$\langle P \rangle = \frac{2\pi}{\hbar\omega} \frac{|\langle c | \Delta V | t \rangle|^2}{\hbar\bar{\nu}} \left(\frac{\pi E_B}{kT} \right)^{1/2} e^{-E_B/kT}. \quad (45)$$

During each period of vibration with $E_Q > E_B$ the level will be crossed twice. Let us neglect the interference of the two contributions to a_t resulting from the two crossings. We will discuss this interference in Sec. III C3. The capture cross section is then found by multiplying $2\langle P \rangle$ by the vibrational frequency and dividing by the incident electron flux $\langle v \rangle/\Omega$. The angular frequency ω cancels out and

$$\sigma_c = \frac{\Omega |\langle c | \Delta V | t \rangle|^2}{\hbar \langle v \rangle \hbar\bar{\nu}} \left(\frac{4\pi E_B}{kT} \right)^{1/2} e^{-E_B/kT}. \quad (46)$$

This equation agrees exactly with Eq. (28) for σ_c

derived in Sec. III B.

The terms in Eq. (46) are readily interpreted. $e^{-E_B/kT}$ is the probability that mode Q has an energy greater than E_B in Fig. 5(b). The average value of $(E_M^2 - \hbar^2\bar{\nu}^2)^{-1/2}$ for vibrations with $E_Q > E_B$ is $(\pi E_B/kT)^{1/2} (\hbar\bar{\nu})^{-1}$. If we define \bar{E}_M by the value of E_M satisfying this average

$$\bar{E}_M^2 - \hbar^2\bar{\nu}^2 \equiv (kT/\pi E_B) \hbar^2\bar{\nu}^2 = 4S\hbar\omega kT/\pi, \quad (47)$$

where we have used Eq. (29) to eliminate $\hbar\bar{\nu}$ and E_B . Substituting Eq. (47) into Eq. (38) we can define an average value of ΔE , which we denote as $\Delta\bar{E}$:

$$\Delta\bar{E} = [4\pi(S\hbar\omega)(\hbar\omega)^2 kT]^{1/4}. \quad (48)$$

$S\hbar\omega$ is greater than $\hbar\bar{\nu}$ for centers with large electron-phonon coupling. As an example of such a center let $S\hbar\omega = 2\hbar\bar{\nu}$, $\hbar\bar{\nu} = 0.4$ eV, and $\hbar\omega = kT = 0.025$ eV, then $\Delta\bar{E} = 0.11$ eV. It is also useful to calculate $\bar{E}_M - \hbar\bar{\nu}$. Expressing $\bar{E}_M^2 - \hbar^2\bar{\nu}^2 \approx 2\hbar\bar{\nu}(\bar{E}_M - \hbar\bar{\nu})$ we find from Eq. (18)

$$\bar{E}_M - \hbar\bar{\nu} = 4S\hbar\omega kT/2\pi\hbar\bar{\nu}. \quad (49)$$

For the same values of parameters we find $\bar{E}_M - \hbar\bar{\nu} = 0.031$ eV. This implies that for the typical vibrations which contribute to capture, the turning point of E_t occurs close to the level crossing, so that the LZ approach in which \dot{E}_t is assumed constant in the crossing region ($|E_t - E_c| < \Delta E$) is not valid. However, in Sec. III C3, we will show that Eq. (46) holds in the strong-coupling-high-temperature limit even when more general sinusoidal motion occurs near the crossing.

2. Breakdown of the adiabatic approximation near a level crossing

It is interesting to compare $a_t(x)$ [Eq. (39)] with the adiabatic solution for $a_t(x)$, which we will denote by $a_A(x)$. $a_A(x)$ can be found by integrating Eq. (35a) by parts and keeping only the first term. The additional terms depend on $(d/dt)[\langle t | \Delta V | c \rangle / (E_t - E_c)]$ and can be regarded as nonadiabatic corrections:

$$a_A = \frac{\langle t | \Delta V | c \rangle}{E_c - E_t} \exp \left(i \int \frac{(E_t - E_c)}{\hbar} dt \right) = -(\langle t | \Delta V | c \rangle / \Delta E x) e^{i\pi x^2/2}. \quad (50)$$

The asymptotic expansion of $C(x) + iS(x)$ for $|x| \gtrsim 1$ is

$$C(x) + iS(x) = \pm \frac{1}{2}(1 + i) + (1/\pi x i) \times e^{i\pi x^2/2} (1 - i/\pi x^2 + \dots), \quad (51)$$

where the positive and negative terms hold for positive and negative values of x , respectively.

Evaluating Eq. (39) with this expansion we find

$$\begin{aligned} a_t(x) &= a_A(x)(1 - i/\pi x^2 + \cdots), \quad x \lesssim -1, \\ a_t(x) &= a_A(x)(1 - i/\pi x^2 + \cdots) \\ &\quad + (\langle t | \Delta V | c \rangle / \Delta E) \pi (1 - i), \quad x \gtrsim 1. \end{aligned} \quad (52)$$

Figure 6 shows $|a_t(x)|^2$ and $|a_A(x)|^2$ throughout the crossing region.

The increase in amplitude of $a_t(x)$ modifies the wave function in two ways. The part of $a_t(x)$ that is proportional to $e^{i\pi x^2/2}$ modifies $|c\rangle e^{-iE_c t/\hbar}$ by mixing of $|t\rangle$ and $|c\rangle$. The part of a_t with a constant phase factor contributes to

$$|t\rangle \exp\left(-i \int \frac{E_t dt}{\hbar}\right)$$

resulting in a probability of transitions from the initial state $|c\rangle$ to state $|t\rangle$. In the crossing ($|x| \leq 1$) these two parts of $a_t(x)$ have essentially the same phase factor and cannot be separated. For $x > 1$ the beating of these two contributions causes the oscillations in Fig. 6.

Figure 6 shows that the adiabatic approximation a_A is a good approximation for $x \lesssim -\frac{1}{2}(E_c - E_t \approx 0.06 \text{ eV})$ but differs greatly from a_t for larger values of x . Nearer to the crossing, $|a_A|^2 - 1$, whereas $|a_t(x)|^2 \approx P_{LZ}$, an infinitesimal quantity. Consequently $|a_A|^2/P_{LZ} \rightarrow \infty$ in Fig. 6.

Up till now we have neglected those parts of Eq. (5) which couple the bound state $|t\rangle$ to the other continuum states $|c'\rangle$. This coupling should have two effects. As long as the bound state is greater than $\approx 0.06 \text{ eV}$ from the continuum states, the coupling will merely cause adiabatic modifications of the bound and continuum states. These can be taken into account by assuming the states are adiabatic up to $Q = Q_1$, where the bound state is $\epsilon_1 \approx \frac{1}{2}\Delta E \approx 0.06 \text{ eV}$ below the continuum. This assumption affects the calculation of $|\langle c | \Delta V | t \rangle|^2$ carried out in Sec. III D. However, we will see that $|\langle c | \Delta V | t \rangle|^2$ is not very sensitive to the choice of ϵ_1 .

The other effect of coupling $|t\rangle$ to the continuum of levels is to cause a decrease in $|a_t|^2$, due to transitions of the captured electron into other continuum states crossed after capture. These transitions change the capture cross section from σ_c to

$$\sigma = \sigma_c P_{tt},$$

where P_{tt} is the probability that the captured electron is not reemitted after capture, prior to Q returning to Q_1 . An approximate calculation of P_{tt} will be carried out in Sec. III E. It is shown there that P_{tt} is of order $\frac{1}{2}$. Hence reemission is significant but it causes little change in the capture cross section.

3. Calculation of σ_c for sinusoidal motion of Q

The calculation of σ_c [Eq. (46)] in Sec. III C 1 was valid only for vibrations of large amplitude, where the turning point occurred far above the crossing. We will now calculate σ_c for general sinusoidal motion described by Eq. (31). We begin with Eq. (35), where $\varphi(t)$ is given by

$$\varphi(t) = (E_M/\hbar\omega) \sin(\omega t) - (h\bar{\nu}/\hbar\omega)(\omega t) \quad (53)$$

and

$$a(t_1) = \frac{\langle t | \Delta V | c \rangle}{i\hbar} \int_{-t_1}^{t_1} e^{i\varphi(t)} d(t). \quad (54)$$

Since the contributions to this integral come primarily from the level crossings where $E_t = E_c$, the integral is essentially unchanged if we extend the limits of integration to $\pm t_1 = \pm \pi/\omega$. Let us also define

$$z \equiv E_M/\hbar\omega, \quad (55)$$

$$\nu \equiv h\bar{\nu}/\hbar\omega. \quad (56)$$

Then

$$\begin{aligned} a_t(t_1) &= \frac{\langle t | \Delta V | c \rangle}{i\hbar\omega} \int_{-\pi}^{\pi} e^{i[z \sin(\omega t) - \nu \omega t]} d(\omega t) \\ &= 2\pi (\langle t | \Delta V | c \rangle / i\hbar\omega) J_\nu(z), \end{aligned} \quad (57)$$

where $J_\nu(z)$ is the Bessel function of order ν defined by

$$J_\nu(z) = \frac{1}{\pi} \int_0^\pi \cos(z \sin x - \nu x) dx. \quad (58)$$

The transition probability for capture occurring during each vibrational period is then

$$P_{ct} = [4\pi^2 |\langle c | \Delta V | t \rangle|^2 / (\hbar\omega)^2] [J_\nu(z)]^2. \quad (59)$$

For a typical center $\hbar\omega = 0.025 \text{ eV}$, $h\bar{\nu} = 0.4 \text{ eV}$, so that $\nu = 16$. The vibrations contributing most to capture transitions have $E_M \approx h\bar{\nu}$. Therefore $z \approx \nu$ and both z and ν are much greater than unity. Under these conditions we can expand $\sin x$ about $x = 0$ in the integral for $J_\nu(z)$ and extend the limit of the integral to ∞ . Then

$$\begin{aligned} J_\nu(z) &\approx \frac{1}{\pi} \int_0^\infty \cos[(z - \nu)x - \frac{1}{6}zx^3] dx \\ &= (2/z)^{1/3} \text{Ai}((\nu - z)(2/z)^{1/3}) \\ &= (\hbar\omega/\Delta E') \text{Ai}(-y), \end{aligned} \quad (60)$$

where

$$\Delta E' = [\frac{1}{2}E_M(\hbar\omega)^2]^{1/3} \approx [\frac{1}{2}h\bar{\nu}(\hbar\omega)^2]^{1/3}, \quad (61)$$

$y = (E_M - h\bar{\nu})/\Delta E'$ and $\text{Ai}(-y)$ is the Airy function. P_{ct} becomes

$$P_{ct} = [4\pi^2 |\langle c | \Delta V | t \rangle|^2 / (\Delta E')^2] \text{Ai}^2(-y). \quad (62)$$

For the above values of $\hbar\omega$ and $h\bar{\nu}$, $\Delta E = 2\hbar\omega = 0.05$ eV. For $y \geq 1$

$$\text{Ai}^2(-y) \approx \pi^{-1} y^{-1/2} \sin^2(\frac{2}{3}y^{3/2} + \frac{1}{4}\pi) \quad (63)$$

and

$$\begin{aligned} P_{ct} &\approx \frac{\langle c | \Delta V | t \rangle^2}{(\Delta E)^2} \frac{4\pi}{(y)^{1/2}} \sin^2(\frac{2}{3}y^{3/2} + \frac{1}{4}\pi) \\ &= 4P_{LZ} \sin^2(\frac{2}{3}y^{3/2} + \frac{1}{4}\pi), \end{aligned} \quad (64)$$

where P_{LZ} is the single pass transition probability given by the LZ theory given by Eq. (41), with $|E_t|$ given by Eq. (37).

P_{ct} and $2P_{LZ}$ are plotted in Fig. 7. The sinusoidal behavior of P_{ct} at large E_M results from the interference of the two contributions to a_t coming from the double crossing of level c by level t . P_{LZ} appears to be a good approximation to P_{ct} , averaged over these oscillations for $E_M - h\bar{\nu} > \Delta E'$. Transitions begin when the energy of the bound state at the turning point E_M is within $\Delta E'$ of the crossing and transitions are maximum when the turning point occurs $\Delta E'$ above the crossing. For a typical center $\hbar\omega = 0.025$ eV, $E_M \approx h\bar{\nu} = 0.4$ eV $= 16\hbar\omega$, according to Eq. (61), $\Delta E' = 2\hbar\omega = 0.05$ eV. Note that for a nearly adiabatic transition, one would expect transitions to occur when the levels are within approximately $|c \langle \Delta V | t \rangle|$ of the crossing. In our case the crossing is nearly sudden and $\Delta E'$ does not depend on this matrix element.

The thermal average of P_{ct} is given by

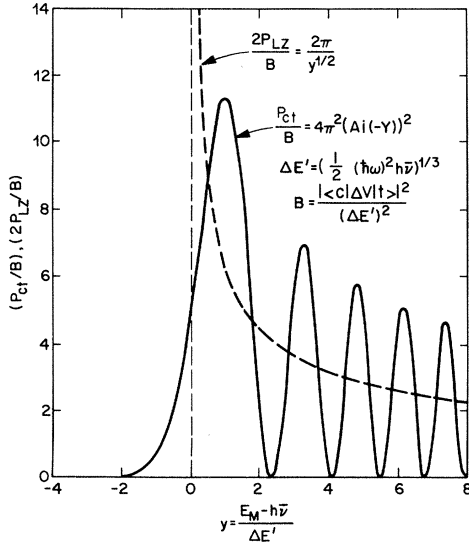


FIG. 7. Double pass transition probability P_{ct} as a function of $E_M - h\bar{\nu}$ for a sinusoidal vibration which varies the level separation as $E_t - E_c = E_M \cos(\omega t - h\bar{\nu})$. $2P_{LZ}$ is the double pass transition probability predicted by the Landau-Zener theory.

$$\langle P_{ct} \rangle = \frac{\sum_{n_c=0}^{\infty} P_{ct}(E_Q) e^{-n_c \hbar\omega / kT}}{\sum_{n_c=0}^{\infty} e^{-n_c \hbar\omega / kT}}. \quad (65)$$

Replacing these sums by integrals, which are valid at high temperatures,

$$\langle P_{ct} \rangle = (kT)^{-1} \int_0^{\infty} dE_Q P_{ct}(E_Q) e^{-E_Q / kT}. \quad (66)$$

Using Eq. (59) for P_{ct} and Eq. (42)

$$z = E_M / \hbar\omega = (h\bar{\nu} / \hbar\omega) (E_Q / E_B)^{1/2} = \nu (E_Q / E_B)^{1/2}, \quad (67)$$

we have

$$\begin{aligned} \langle P_{ct} \rangle &= \frac{4\pi^2 |\langle c | \Delta V | t \rangle|^2}{(\hbar\omega)^2 kT} \int_0^{\infty} dE_Q J_{\nu}^2 \left[\left(\frac{E_Q}{E_B} \right)^{1/2} \nu \right] e^{-E_Q / kT} \\ &= \frac{4\pi^2 |\langle c | \Delta V | t \rangle|^2}{(\hbar\omega)^2} \frac{E_B}{kT} \int_0^{\infty} dx J_{\nu}^2 [(x)^{1/2} \nu] e^{-(E_B / kT) x} \\ &= \frac{4\pi^2 |\langle c | \Delta V | t \rangle|^2}{(\hbar\omega)^2} I_{\nu}(w) e^{-w}, \end{aligned} \quad (68)$$

where I_{ν} is the modified Bessel function of order ν and

$$w = \frac{\nu^2 kT}{2E_B} = \frac{\nu h\bar{\nu}}{2E_B} \frac{kT}{\hbar\omega} = 2\nu \frac{S\hbar\omega}{\hbar\bar{\nu}} \frac{kT}{\hbar\omega}. \quad (69)$$

For $\nu \gg 1$, the asymptotic expansion of $I_{\nu}(w)$ is⁶¹

$$\begin{aligned} I_{\nu}(w) e^{-w} &\approx [(2\pi)^{1/2} (\nu^2 + w^2)^{1/4}]^{-1} \\ &\quad \times \exp[-\nu \sinh^{-1}(\nu/w) - w + (\nu^2 + w^2)^{1/2}]. \end{aligned} \quad (70)$$

For $w \gtrsim \nu$ there is a further simplification. This condition is satisfied at room temperature for large electron-phonon coupling ($S\hbar\omega > h\bar{\nu}$) or at higher temperature for weaker electron-phonon coupling. Under these circumstances

$$I_{\nu}(w) e^{-w} \approx (2\pi w)^{-1/2} e^{-\nu^2 / 2w} \quad (71)$$

and

$$\langle P_{ct} \rangle \approx 4\pi^2 \left(\frac{E_B}{\pi kT} \right)^{1/2} \frac{|\langle c | \Delta V | t \rangle|^2}{h\bar{\nu} \hbar\omega} e^{-E_B / kT}. \quad (72)$$

The cross section σ_c is given by

$$\begin{aligned} \sigma_c &= (\omega / 2\pi) \langle P_{ct} \rangle (\Omega / \langle \nu \rangle) \\ &= \Omega \left(\frac{4\pi E_B}{kT} \right)^{1/2} \frac{|\langle c | \Delta V | t \rangle|^2}{\hbar \langle \nu \rangle h\bar{\nu}} e^{-E_B / kT}. \end{aligned} \quad (73)$$

This formula is in complete agreement with Eq. (46) derived using the LZ formula and with Eq. (28) derived using a quantized lattice.

D. Evaluation of the matrix element $\langle c|\Delta V|t\rangle$ for a neutral center

We want to calculate the matrix element $\langle c|\Delta V|t\rangle$, where $|c\rangle$ and $|t\rangle$ are the adiabatic states of a spherical square well of depth V_0 with a bound state $\epsilon_1 \approx 0.06$ eV below the continuum. We assume the radius of the well b is of order the nearest-neighbor separation (2.36 Å for GaP). The radius a of the bound state [defined by Eq. (75) below] is given by

$$a = (\hbar^2/2m^* \epsilon_1)^{1/2}. \quad (74)$$

For $m^* = 0.4m_0$, which is appropriate for GaP, $a = 12.6$ Å and $b/a = 0.19$. We will assume $b/a \ll 1$, $kb \ll 1$, and $ka \approx 1$, where k is the wave vector of the free carrier. Under these assumptions the wave functions can be readily calculated. The continuum state can be expanded in partial waves of angular momentum l . For low-energy electrons $kb \ll 1$, only the $l=0$ component has an appreciable matrix element. We will neglect $l \neq 0$ partial waves. Then $|c\rangle$ and $|t\rangle$ are of the form $u_i(r)/r$, $i=c, t$, where

$$u_t = \begin{cases} A_t \sin(K_t r), & r < b, \\ A_t \sin(K_t b) e^{-(r-b)/a}, & r > b, \end{cases} \quad (75)$$

$$u_c = \begin{cases} A_c \sin(K_c r), & r < b, \\ \sin(kr + \delta)/k\Omega^{1/2}, & r > b, \end{cases} \quad (76)$$

where K_t and K_c are defined by the relations $K_t^2 \equiv (2m^*/\hbar^2)(V_0 - \epsilon_1)$ and $K_c^2 \equiv (2m^*/\hbar^2)V_0 + k^2$. Here well depth V_0 is large compared to ϵ_1 and $(\hbar^2/2m^*)k^2$. A_t is determined by normalization and is approximately

$$A_t \approx (2\pi a)^{-1/2}. \quad (77)$$

δ is the $l=0$ phase shift. For low-energy electrons

$$\delta = \pi - ka_c, \quad (78)$$

where parameter a_c defined by Eq. (78) is the scattering length. The requirement that u_c and du_c/dr be continuous at $r=b$ leads to

$$K_c \cos K_c b = k \cot(kb + \delta) = -k \cot[k(a_c - b)] \quad (79)$$

and

$$A_c = \sin[k(a_c - b)]/k\Omega^{1/2} \sin(K_c b). \quad (80)$$

A similar requirement for the bound state leads to

$$K_t \cot(K_t b) = -1/a. \quad (81)$$

Using the definitions of K_t and K_c and Eq. (74) lead to

$$K_c^2 = K_t^2 + 1/a^2 + k^2 \approx K_t^2. \quad (82)$$

K_t and K_c are almost equal. Because of this near equality, we can equate the right-hand sides of

Eqs. (79) and (81), which results in

$$ka = \tan[k(a_c - b)]. \quad (83)$$

Assuming $k(a_c - b) \lesssim 1$, $\tan[k(a_c - b)] \approx k(a_c - b)$, Eq. (83) becomes

$$a \approx a_c - b. \quad (84)$$

Using $\sin(K_c b) \approx 1$ and $\sin[k(a_c - b)] \approx k(a_c - b)$, Eq. (80) becomes

$$A_c = (a_c - b)\Omega^{-1/2} \approx a\Omega^{-1/2}. \quad (85)$$

The matrix element is

$$\begin{aligned} \langle c|\Delta V|t\rangle &= 4\pi A_c A_t (\Delta V_0) \int_0^b \sin(K_c r) \sin(K_t r) dr \\ &\approx 2\pi A_c A_t b (\Delta V_0) \approx (2\pi a)^{1/2} b (\Delta V_0). \end{aligned} \quad (86)$$

We have used $K_c b \approx K_t b \approx \frac{1}{2}\pi$ as approximating the integral by $\frac{1}{2}b$. Here ΔV_0 denotes the change in the depth of the potential well required to change E_t by ϵ_1 . That is,

$$\epsilon_1 = \langle t|\Delta V|t\rangle \approx (\Delta V_0) b/a. \quad (87)$$

Finally combining Eqs. (86) and (87) we have

$$\begin{aligned} \Omega |\langle c|\Delta V|t\rangle|^2 &\approx (2\pi a^3) \epsilon_1^2 \\ &= 2\pi (\hbar^2/2m^*)^{3/2} \epsilon_1^{1/2}. \end{aligned} \quad (88)$$

This equation is appealing because the matrix element does not depend on either the range or depth of the potential well and it depends only insensitively on ϵ_1 . Note that at $r=b$,

$$|c\rangle = A_c \sin(K_c b)/b\Omega^{1/2} \approx (a/b)\Omega^{-1/2}, \quad (89)$$

so that in the vicinity of the potential well the amplitude of $|c\rangle$ is enhanced by (a/b) over the amplitude of a plane wave. Approximating the continuum states as plane waves underestimates $|\langle c|\Delta V|t\rangle|^2$ and leads to an expression for σ_c that is a sensitive function of both b and a . This error was made in our earlier publication.³² We are grateful to the referee of this paper for pointing out this error.

Using Eq. (88), Eq. (28) for σ_c becomes

$$\sigma_c = \left(\frac{4\pi E_B \epsilon_1}{kT \hbar^2 v^2} \right)^{1/2} \frac{2\pi (\hbar^2/2m^*)^{3/2}}{\hbar \langle v \rangle} e^{-E_B/kT}. \quad (90)$$

Using

$$\langle v \rangle = (8kT/\pi m^*)^{1/2}$$

and $E_B = \hbar^2 v^2/4S\hbar\omega$ (Eq. 29), we find

$$\sigma_c = \left(\frac{\epsilon_1}{S\hbar\omega} \right)^{1/2} \frac{\pi^2}{4kT} \frac{\hbar^2}{m^*} e^{-E_B/kT}. \quad (91)$$

We can approximate $(kT)^{-1}$ near $T = T_R = 300$ K as

$$(kT)^{-1} \approx (kT_R)^{-1} e^{-1} e^{kT/kT_R}.$$

Then

$$\sigma_c = \sigma_{\infty c} e^{-E_{\infty c}/kT}, \quad (92)$$

where

$$\sigma_{\infty c} = (\epsilon_1/S\hbar\omega)^{1/2} (\pi^2/2e) (\hbar^2/2m^*kT_R) \quad (93)$$

and

$$E_{\infty c} = E_B - kT_R. \quad (94)$$

Using, as in Sec. III C, the typical values $S\hbar\omega = 2E_c$, $E_c = 0.4$ eV, $\epsilon_1 = 0.06$ eV, $m^* = 0.4m_0$, and $kT_R = 0.025$ eV, we estimate

$$\begin{aligned} \sigma_{\infty c} &= 6.9 \times 10^{-14} (\epsilon_1/S\hbar\omega)^{1/2} \text{ cm}^2 \\ &= 1.9 \times 10^{-14} \text{ cm}^2. \end{aligned} \quad (95)$$

We can also evaluate coefficient A in Eq. (20)

$$\begin{aligned} A_c &= (2\pi\Omega/\hbar\langle v \rangle) |\langle c | \Delta V | t \rangle|^2 \\ &= (\epsilon_1\pi^5/kT)^{1/2} (\hbar^2/2m^*). \end{aligned} \quad (96)$$

Using $m^* = 0.4$ and $kT = 0.025$ eV,

$$A_c = 2.6 \times 10^{-14} \text{ cm}^2 \text{ eV}. \quad (97)$$

E. Approximate calculation of the probability of reemission

The correct calculation of the capture cross section, including reemission of the bound electron after capture, requires solution of Eq. (34), describing the coupling of the bound state with the continuum of free states. This is a difficult mathematical problem and beyond the scope of this paper. Instead we will make a crude estimate of P_{tt} , the probability that the electron will not be reemitted after capture, based on a physical picture illustrated in Fig. 8(b).

We will assume for simplicity that the captured electron can only be reemitted into those levels crossed after capture. According to LZ, the probability that the bound electron is not reemitted when crossing level c' is $e^{-P_{LZ}}$, where P_{LZ} is the single crossing transition probability given by Eq. (41) with c replaced by c' . P_{tt} is the product of these probabilities

$$P_{tt} = \prod_{c'} e^{-P_{LZ}} = \exp\left(-\sum_{c'} P_{LZ}\right), \quad (98)$$

where the sum extends over all levels c' crossed after capture. While P_{LZ} is infinitesimal, $\sum_{c'} P_{LZ}$ is finite and leads to a reemission process similar to that occurring in a nearly adiabatic crossing. This similarity is illustrated in Fig. 8.

We can write $\sum_{c'} P_{LZ}$ as an integral

$$S \equiv \sum_{c'} P_{LZ} = \int \frac{dN_c}{dE} \frac{2\pi}{\hbar} \frac{|\langle c' | \Delta V | t \rangle|^2}{|\dot{E}_t|} dE_{c'}. \quad (99)$$

The integral ranges over the energy of all states crossed after capture. If capture occurs before

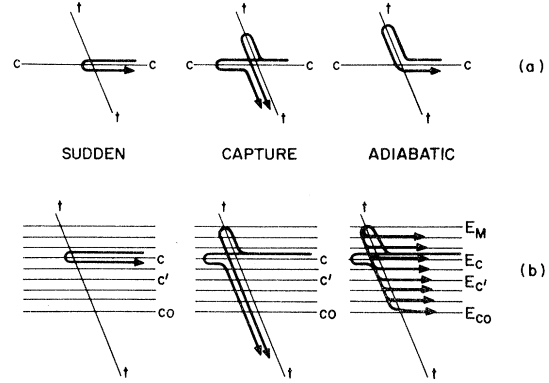


FIG. 8. Transitions occurring during a double passage. In sudden passage no transitions occur. In adiabatic passage two transitions occur. Capture takes place if a single transition occurs. (a) The crossing of two levels; (b) shows the analogous cases for a bound state crossing through a continuum of levels.

the turning point E_M , the integral is the sum of two terms with limits of integration E_c and E_M and E_{c_0} and E_M , where E_{c_0} is the lowest energy in the conduction band. If capture occurs after the turning point, the integral ranges from E_{c_0} to E_c . For average vibrations contributing to capture, we have from Eq. (49) $\bar{E}_M - E_c = (4S\hbar\omega/2\pi\hbar\bar{v})kT = (4/\pi)kT$ for $S\hbar\omega = 2\hbar\bar{v}$ a typical value with strong electron phonon coupling. The average energy of the incident carrier is $\bar{E}_c - E_{c_0} = \frac{3}{2}kT$.

To gain some feeling for the typical value of S while not getting bogged down in difficult integrations, let us calculate a representative value of S , which we shall call \bar{S} in which the integration ranges from E_{c_0} to the average turning point \bar{E}_M ,

$$\bar{E}_M - E_{c_0} = \left(\frac{3}{2} + 2S\hbar\omega/\pi\hbar\bar{v}\right)kT. \quad (100)$$

In calculating $|\dot{E}_t|$ in Eq. (99), we must take into account that after capture the lattice is moving along the bound-state configuration-coordinate diagram. In analogy with Eq. (37)

$$|\dot{E}_t| = \omega[(E'_M)^2 - (E'_{c'})^2]^{1/2}, \quad (101)$$

where E'_M and $E'_{c'}$ are the energies of the bound state at the turning point and the energy of free state c' , both measured relative to the energy of the bound-state energy at \bar{Q} [Fig. 5(b)]. We can reexpress $|\dot{E}_t|$ as

$$\begin{aligned} |\dot{E}_t| &\approx \omega(2E'_{c'})^{1/2}(E'_M - E'_{c'})^{1/2} \\ &= \omega[2(2S\hbar\omega + \hbar\bar{v})]^{1/2}(E_M - E_{c'})^{1/2}, \end{aligned} \quad (102)$$

where we have approximated $E'_{c'}$ by E'_{c_0} and used $E'_M - E'_{c'} = E_M - E_{c_0}$. The density of states is

$$\frac{dN_c}{dE} = \frac{\Omega}{(2\pi)^2} \left(\frac{2m^*}{\hbar^2}\right)^{3/2} (E_{c'} - E_{c_0})^{1/2}. \quad (103)$$

Using Eqs. (99), (102), and (103), \bar{S} is

$$\bar{S} = \frac{\Omega |\langle c | \Delta V | t \rangle|^2}{2\pi \hbar \omega [2(h\bar{\nu} + 2S\hbar\omega)]^{1/2}} \left(\frac{2m^*}{\hbar^2} \right)^{3/2} \times \int_{E_{c0}}^{\bar{E}_M} \frac{(E_{c'} - E_{c0})^{1/2}}{(E_M - E_{c'})^{1/2}} dE_{c'}. \quad (104)$$

The integral equals $\frac{1}{2} \pi (\bar{E}_M - E_{c0})$. Evaluating $\Omega |\langle c | \Delta V | t \rangle|^2$ with Eq. (88) and $\bar{E}_M - E_{c0}$ with Eq. (100)

$$\bar{S} = \frac{\pi}{2} \left(\frac{\epsilon_1}{2(h\bar{\nu} + 2S\hbar\omega)} \right)^{1/2} \left(\frac{3}{2} + \frac{2S\hbar\omega}{\pi E_c} \right) \frac{kT}{\hbar\omega}. \quad (105)$$

For typical values $\hbar\omega = 0.025$ eV, $\epsilon_1 = 0.06$ eV, $E_c = 0.4$ eV, $S\hbar\omega = 2E_c$, and $kT = 0.025$ eV we find $\bar{S} = 0.68$. For a carrier captured at the turning point

$$P_{tt} = e^{-\bar{S}} = 0.50.$$

On the average, the turning point occurs an amount $\bar{E}_M - E_c$ above level c . For such an average vibrational motion there are two values of S depending on whether capture occurs before or after the turning point. The average of the two contributions to P_{tt} is

$$\bar{P}_{tt} = \frac{1}{2} (e^{-\bar{S}(2-I)} + e^{-\bar{S}I}), \quad (106)$$

where

$$I = \left[\frac{1}{2} \pi (E_M - E_{c0}) \right]^{-1} \int_{E_{c0}}^{\bar{E}_c} \frac{(E_{c'} - E_{c0})^{1/2}}{(E_M - E_{c'})^{1/2}} dE_{c'}, \\ = (2/\pi)(\theta - \sin\theta \cos\theta) \quad (107)$$

and

$$\theta = \sin^{-1}[(\bar{E}_c - E_{c0})/(\bar{E}_M - E_{c0})]^{1/2}. \quad (108)$$

For $S\hbar\omega = 2h\bar{\nu}$, $(\bar{E}_c - E_{c0})/(\bar{E}_M - E_{c0}) = 0.54$, $\theta = 47^\circ$, and

$$I = 0.21, \\ \bar{P}_{tt} = \frac{1}{2} (e^{-1.79\bar{S}} + e^{-0.21\bar{S}}) = 0.58. \quad (109)$$

\bar{S} is proportional to kT , causing \bar{P}_{tt} to decrease with temperature. Near room temperature we can express the temperature dependence of \bar{P}_{tt} as

$$\bar{P}_{tt} = 0.35 e^{+0.012 \text{ eV} / kT}. \quad (110)$$

The capture cross section for a neutral center is

$$\sigma = \sigma_c \bar{P}_{tt} = \sigma_\infty e^{-E_\infty / kT}. \quad (111)$$

From Eqs. (94) and (95), we have

$$\sigma_\infty = 0.35(\sigma_\infty)_c = 6.6 \times 10^{-15} \text{ cm}^2, \quad (112)$$

$$E_\infty = E_{\infty c} - 0.012 \text{ eV} = E_B - 0.037 \text{ eV}. \quad (113)$$

Similarly

$$\sigma = Af(0), \quad (114)$$

where

$$A = \bar{P}_{tt} A_c = 1.5 \times 10^{-14} \text{ cm}^2 \text{ eV}. \quad (115)$$

F. Discussion

In Secs. III A–III E we have carried out a detailed calculation of MPE capture using a model that had the following limitations: the impurity was neutral before capture; the wave functions of the free and bound states were describable in a one-band effective-mass approximation; a single vibrational displacement Q caused both the crossing of the free and bound states and the transition between these states; and E_t was assumed linear with Q . Obviously this simple model does not cover all the complex situations that arise in studying capture and recombination for a variety of different impurities. These include capture by charged centers, capture in which the bound state and the free state have different symmetry, and nonlinearities in E_t vs Q . We will not carry out calculations for these cases but merely make a few speculative remarks.

In a number of cases the bound state has a different symmetry than the free-carrier state. For example, consider a substitutional impurity with tetrahedral symmetry T_d . A bound-electron state is likely to have irreducible representation Γ_6 of group T_d . Symmetric Γ_1 vibrations which alter the depth of the potential well will not change the symmetry of the state. The bound state will recombine with holes at the top of the valence band which have irreducible representation Γ_8 . In first order, the bound-electron state and the free-hole state will be coupled by Γ_3 , Γ_4 , Γ_5 vibrations but not by Γ_1 vibrations.⁶²

Cases such as this may be better treated by a model in which the impurity is coupled by two lattice modes. A symmetric mode Q_1 which alters the well depth, causes the motion of the bound level relative to the free-carrier bands, and a second mode of different symmetry Q_2 which couples the bound state $|t\rangle$ and the free state $|v\rangle$. If the electron-lattice interaction is

$$\mathcal{H}_{EL} = \left(\frac{\partial V}{\partial Q_1} \right) Q_1 + \left(\frac{\partial V}{\partial Q_2} \right) Q_2, \quad (116)$$

then we expect

$$\sigma \approx \frac{2\pi\Omega}{\hbar\langle v \rangle} \left| \langle t | \frac{\partial V}{\partial Q_2} | v \rangle \right|^2 \langle Q_2^2 \rangle f(0), \quad (117)$$

where $f(h\nu)$ is the line shape for thermal broadening of optical capture transitions by mode Q_1 . The cross section is again of the form $\sigma = Af(0)$.

An electron trapped at a neutral center will recombine with a hole attracted to the center by Coulomb attraction. The hole can occupy a 1S

state, enhancing the charge density near the potential well. For GaP, it has been shown for the Cd-O, Zn-O,⁶³ and N-N pairs⁶⁴ that the 1S hole state has a binding energy of approximately 35–40 meV. The thermally averaged occupancy of this state leads to an enhancement η of the hole charge density near the potential well relative to the average hole density p , where

$$\eta = g e^{E_{1S}/kT} |\varphi_{1S}(0)|^2 / N_v. \quad (118)$$

We estimate $g=4$, $E_{1S}=0.035$ eV, $|\varphi_{1S}(0)|^2 = 2 \times 10^{19}/\text{cm}^3$, and $N_v = 2 \times 10^{19}/\text{cm}^3$ and find $\eta \approx 16$ at room temperature. η decreases rapidly with temperature because of the exponential factor and because $N_v \propto T^{3/2}$. Near room temperature η can be fitted as

$$\eta = 0.88 e^{+0.073/kT}.$$

Thus Coulomb attraction causes an enhancement of σ at room temperature, but no enhancement of σ_∞ .

Up till now we have assumed for simplicity that E_t varies linearly with Q in Fig. 5(a). This would be the case if the wave function $|t\rangle$ did not change with Q . However the adiabatic change of $|t\rangle$ with Q (valid throughout the band gap except within ≈ 0.06 eV of the band edges) produces nonlinearities in E_t vs Q which increase E_B for carrier capture and decrease E_B for carrier recombination. This is illustrated in Fig. 9 where we have plotted the bound-state energy E_t versus well depth for the spherical square well. The linear curve is a linear approximation made with $E_t = 0.4$ eV. dE_t/dQ is proportional to dE_t/dV_0 and,

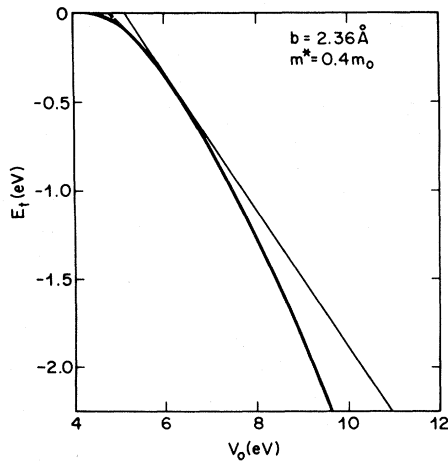


FIG. 9. Binding energy E_t vs well depth V_0 for the spherical square well of radius b . The dashed line shows the deviation from the adiabatic approximation for $|E_t| \lesssim 0.06$ eV. The straight curve is the linear approximation to E_t made using dE_t/dV_0 at $E_t = -0.4$ eV.

$$\frac{dE_t}{dV_0} = \int_0^b 4\pi r^2 dr |\psi_t(r)|^2. \quad (119)$$

That is, dE_t/dV_0 equals the probability that the bound carrier is within the potential well of radius b . This probability increases with binding energy giving the observed nonlinearities. The increase in m^* with binding energy would also increase this nonlinearity. Additional nonlinearities will result from the softening of lattice modes by bound carriers, discussed by Heine and Henry.⁶⁵

These nonlinearities will be much more extreme in the case of MPE capture by a deep donor (or acceptor) because the probability that the electron is within the potential well rapidly decreases with decreasing binding energy. For example, Heine and Henry⁶⁵ have made an approximate estimate of the charge density within radius b versus binding energy for neutral and Coulomb attractive centers. They find for electron traps in GaP that as E_t decreases from 0.4 to 0.06 eV the fraction of charge within the central cell decreases from 0.64 to 0.33 for a neutral center and from 0.4 to 0.014 for a Coulomb attractive center.

Evidence that these nonlinearities substantially affect the capture cross sections of the Zn-O and O centers in GaP is presented in Sec. IV.

IV. COMPARISON OF THEORY AND EXPERIMENT

A. Temperature dependence of the capture cross sections

The temperature dependences of the capture cross sections in Fig. 2 all show the exponential behavior expected with temperature. All of the cross sections except one extrapolate exponentially to nearly the same value $\sigma_\infty = 10^{-14} - 10^{-15}$ cm² at high temperatures. The exception is the cross section for electron capture by state 2 of O in GaP. A possible reason for this exception will be discussed in Sec. IV D. We hasten to point out that not all cross sections that we have measured exhibit an increase with temperature. Some notable exceptions are electron capture into state 1 of O in GaP,³³ and hole capture by Fe and Cr in GaAs.³⁴ In all of these cases the measured cross sections are substantially less than 10^{-15} cm² and decrease slowly with increasing temperature. We assume that another nonradiative process causes capture in these cases.

The theory of Sec. III [Eqs. (95) and (110)] for capture of a carrier by an attractive neutral center, predicts a value of $\sigma_\infty \approx 6 \times 10^{-15}$ cm² which has the same order of magnitude as values of $\sigma_\infty = 10^{-14} - 10^{-15}$ cm² observed for a variety of centers in Fig. 2. The theory of SK also predicts values of σ_∞ in this range for neutral and Coulomb attractive centers. We should emphasize that both our

theory and that of SK use the effective-mass approximation. Neither theory takes into account that the symmetry of the level may be different from that of the band state. However we do not expect that additional complexities present in the actual data (which encompasses capture and recombination transitions, transition elements, and unknown centers) can alter the relations $\sigma = \sigma_\infty e^{-E_\infty/kT}$ or $\sigma = Af(0)$. These complexities would most likely contribute to changes primarily in the predicted value of σ_∞ and A .

B. Capture of an electron by the Zn-O center in GaP

The Zn-O center in GaP is a well understood neutral center for which both the recombination luminescence and electron-capture cross section are accurately known. The Zn-O center has been studied both in absorption and emission by Cuthbert *et al.*⁶⁶ They established the energy of the exciton bound to the Zn-O center at helium temperature to be approximately 2.02 eV, or 0.319 eV less than the energy gap. Henry *et al.*⁶³ found the binding energy of the hole in the bound exciton to be approximately 0.037 eV. Subtracting this energy from the 0.319 eV we determine that the binding energy of the Zn-O center is $E_0 = 0.282$ eV. This agrees quite well with an ionization energy of 0.285 eV measured by Jayson *et al.*⁴⁸ from thermal emission measurements.

If we neglect nonlinear electron-lattice interactions, then the values of S and $\hbar\omega$ determined for the line shape of the recombination luminescence also describe the line shape for radiative capture $\bar{f}(h\nu)$. The first moment of the emission line shape occurs at about 0.19 eV below the zero-phonon energy (2.02 eV). The full width at half maximum of the emission line shape at 4 K is $\Delta E_{1/2} \cong 0.14$ eV.⁶⁷ In the Gaussian approximation, the second moment of the line $\langle E^2 \rangle = (E_{1/2})^2/8 \ln 2 = (0.059 \text{ eV})^2$. S and $\hbar\omega$ can be calculated from the measured first and second moments using Eqs. (25) and (26). The experimental and theoretical parameters for the Zn-O center are tabulated in Table I. The large value of $S = 10.2$ justifies using the Gaussian line shape Eq. (27) to calculate $f(0)$. The parameters S and $\hbar\omega$ are reasonably close to the values found in earlier fits of the Zn-O luminescence by Morgan *et al.*⁶⁷

The electron capture cross section for the Zn-O center has been measured by Jayson *et al.*⁴⁸ to be $\sigma_n = (2^{+2}_-1) \times 10^{-15} \text{ cm}^2$ at 300 K and by Lang²⁷ to be $(0.9 \pm 0.5) \times 10^{-15} \text{ cm}^2$ at 190 K. These two values lead to an estimate of $\sigma_\infty = (8^{+20}_-6) \times 10^{-15} \text{ cm}^2$.

The theoretical parameters for the Zn-O center are listed in Table I. ϵ_1 and P_{tt} were calculated

TABLE I. Parameters of the Zn-O center in GaP at $T = 300$ K.

Experiment	Theory
$E_0 = 0.282$ eV	Same
$S\hbar\omega = 0.19$ eV	Same
$S(\hbar\omega)^2 = (0.059 \text{ eV})^2$	Same
...	$S = 10.2$
...	$\hbar\omega = 0.0186$ eV
...	$f(0) = 2.6 (\text{eV})^{-1}$
...	$E_B = 0.011$ eV
...	$E_\infty = -0.027$
	$\epsilon_1 = 0.034$ eV
	$P_{tt} = 0.45$
$\sigma_n(300 \text{ K}) = (2^{+2}_-1) \times 10^{-15} \text{ cm}^2$	$\sigma_n(300 \text{ K}) = 23 \times 10^{-15} \text{ cm}^2$
$\sigma_{n\infty} = (8^{+20}_-6) \times 10^{-15} \text{ cm}^2$	$\sigma_{n\infty} = 8 \times 10^{-15} \text{ cm}^2$
	$S\hbar\omega = 0.12^a$
	$E_B = 0.049^a$
	$E_\infty = 0.010^a$
	$\sigma_n(300 \text{ K}) = 7 \times 10^{-15} \text{ cm}^2^a$

^a These values include a correction for nonlinear electron-lattice interactions.

from using $\epsilon_1 = \frac{1}{2}\Delta\bar{E}$ and Eqs. (48) and (106). The value for σ_∞ is in good agreement with experiment. However the theoretical capture cross at room temperature is an order of magnitude too large, and the theory predicts that the cross section will decrease slowly with increasing temperature ($E_\infty < 0$). A possible explanation for these discrepancies is that nonlinearity of $E_t(Q)$ interactions must not be neglected. As discussed in Sec. III E (see Fig. 9) these nonlinear electron-lattice interactions will not effect σ_∞ , but will increase E_B , decreasing the theoretical values of the cross section at lower temperatures.

The nonlinear electron-lattice interaction is conceptually easy to understand. The coupling to the lattice is determined by $S\hbar\omega$. We have fitted this parameter using recombination luminescence. During recombination luminescence, the electron has an average binding energy relative to the conduction band of $E_0 + S\hbar\omega \approx 0.47$ eV (see Fig. 5). To understand capture we need to know the coupling to the lattice as the binding energy decreases from E_0 to ϵ_1 . The average binding energy is $\approx \frac{1}{2}E_0 = 0.14$ eV. According to the estimate of Henry and Heine, the probability that the electron is within the potential well decreases from 0.68 to 0.45 as the binding energy decreases 0.47–0.14 eV. If we assume $S\hbar\omega$ is proportional to the time spent within

the potential well, $S\hbar\omega$ decreases from 0.19 to 0.12 eV. According to Eq. (29) this changes E_B from 0.011 to 0.049 eV and decreases the theoretical value of the cross section at room temperature from 23×10^{-15} to 7×10^{-15} cm², a value that has the same order of magnitude as the measured value.

C. Configuration coordinate diagram for state 2 of O in GaP

The theory of nonradiative capture presented in Sec. III shows that the capture cross sections depend sensitively on the amount of lattice relaxation. If a large energy is dissipated in the transition, large cross sections are only possible if the amount of lattice relaxation associated with the level is substantial. In a complete nonradiative cycle of capture and recombination the level moves across the entire energy gap. This process is only probable if the equilibrium position of the level prior to capture is near the conduction band and after capture is near the valence band. The equilibrium positions of the level can be established by optical emission or absorption experiments.

A striking example is state 2 of O in GaP. This state has a large capture cross section for holes $[(0.3-1.7) \times 10^{-14}$ cm²] and is believed²⁵ to dissipate about 1.35 eV in this transition. The cross section tends to decrease slightly with temperature indicating an extremely small barrier height. We will present evidence that a large lattice relaxation is responsible for this large cross section. Kukimoto *et al.*²⁵ and Henry *et al.*²⁶ established that O in GaP has two bound states, state 1 with one deeply bound electron and state 2 with two deeply bound electrons. Kukimoto *et al.*²⁵ measured the photoionization cross sections of state 1 and state 2. Their interpretation of this data was that state 2 has substantial lattice relaxation while state 1 has only small lattice relaxation.⁶⁸ Later Grimmeiss *et al.*⁶⁹ presented a different interpretation of state 2, based on photoconductivity measurements, which implied that state 2 has little lattice relaxation. Recently Jaros⁷⁰ has calculated the energies of states 1 and 2 of substitutional O_p in GaP. He finds that O will deeply bind both states and that the deep binding of the state 2 electron is due to a substantial rearrangement of the valence electrons.

In order to try to settle the controversy of whether state 2 of O has large lattice relaxation, we have repeated the measurements of the photoionization cross sections and carried them out over a range of temperatures varying from 120 to 400 K. The temperature variation of the cross-sections is crucial. Besides altering the threshold

energies of the cross sections, lattice relaxation also causes substantial thermal broadening which increases with temperature. The optical cross sections are shown in Figs. 10 and 11. The data are consistent with large lattice relaxation of state 2.

The various transitions are defined by the diagrams inserted in these figures. The equilibrium positions of the levels before and after occupation by an electron are shown in the inserts. The energies were determined for state 2 from analysis of the optical cross-section data. For state 1 the energies were determined from luminescence data, a more accurate method, but are consistent with photocapacitance data. The methods of the optical cross-section measurement and the analy-

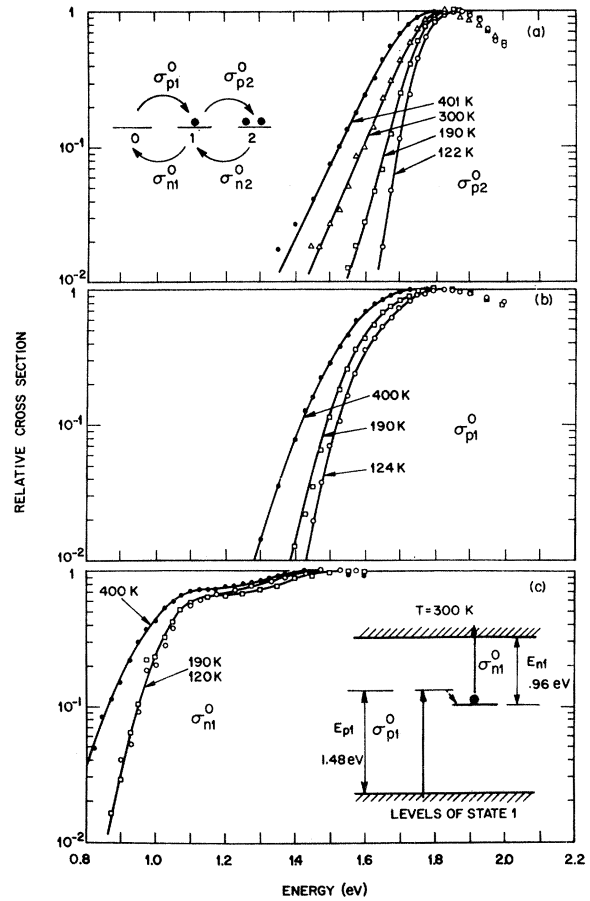


FIG. 10. Optical cross sections σ_{p1}^0 and σ_{n1}^0 of state 1 and σ_{p2}^0 and σ_{n2}^0 of state 2 of O in GaP. Note the small degree of broadening of σ_{n1}^0 and σ_{p1}^0 compared to σ_{p2}^0 and σ_{n2}^0 in Fig. 11. The insert in (a) indicates how the optical transitions change and charge states of the O center. The insert in (c) indicates the energy levels of state 1 before and after lattice relaxation. The energy levels were determined by luminescence and are consistent with the photocapacitance data shown here.

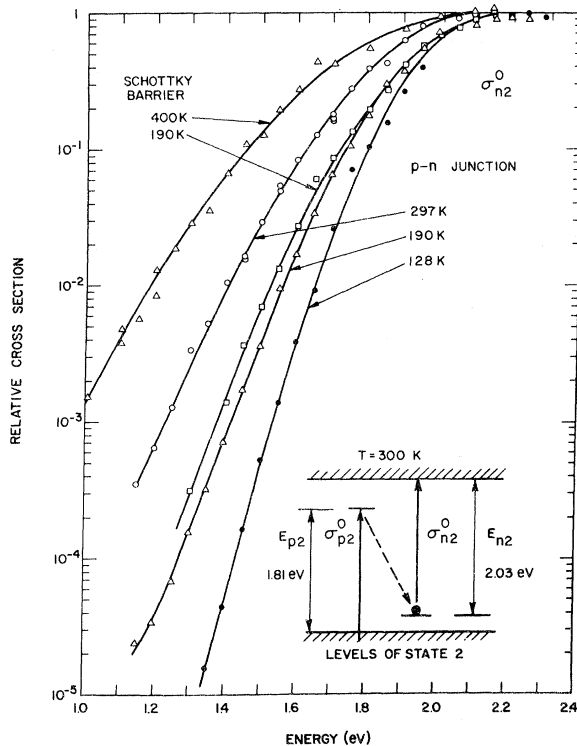


FIG. 11. Photoionization cross section σ_{n2}^0 of state 2 of O in GaP. Note the substantial thermal broadening of this cross section. The change of slope of the 190-K curve near 1.2 eV is due to thermal ionization of the trapped electron. Thermal effects were subtracted from the higher-temperature data. The insert shows the energy levels for state 2 before and after lattice relaxation as determined from analysis of σ_{n2}^0 and σ_{p2}^0 . The diagram indicates a very large drop in the level energy with lattice relaxation.

sis of the threshold energies are briefly discussed in Appendix A. For state 2 these energies were determined by fitting the optical cross sections with Gaussian curves. The fitting parameters are tabulated in Table II. The data for the photoionization energy of state 2, shown in Fig. 11, was taken over a range of up to five decades in order to compare it with the data of Grimmeiss *et al.*⁶⁹ We find no evidence for the 0.65-eV

TABLE II. Parameters determined by fitting the optical cross section σ_{n2}^0 and σ_{p2}^0 of state 2 of O in GaP.

T (K)	\bar{E}_{n2} (eV)	$\langle (E^2)_{n2} \rangle^{1/2}$ (eV)	E_{n2} (eV)	\bar{E}_{p2} (eV)	$\langle (E^2)_{p2} \rangle^{1/2}$ (eV)	E_{p2} (eV)
120	2.18	0.17	2.09	1.84	0.07	1.81
190	2.18	0.21	2.07	1.86	0.10	1.81
300	2.15	0.25	2.03	1.88	0.14	1.81
400	2.10	0.30	1.95	1.88	0.17	1.80

threshold energy or for the structure they observed. A possible explanation of this discrepancy is given in Appendix B.

Figures 10 and 11 show vividly that the phonon broadening of the transitions of state 2 is much greater than the phonon broadening of the transitions of state 1. The threshold data as well as the inserted diagrams interpreting this data also show that the deduced thresholds are consistent with a small change in the energy of state 1 with lattice relaxation (0.20 eV), but a large change in the energy of state 2 (1.56 eV).

The thermal broadening of σ_{n2}^0 is much greater than that of σ_{p2}^0 . According to the simple model depicted in Fig. 5(b), the broadening of the two cross sections should be the same. This asymmetry can be explained by assuming that the lattice frequency decreased after capture of the electron.

A decrease in lattice frequency after capture is also needed to explain the thermal emission data of state 2. The thermal emission rates e_{n1} and e_{n2} for state 1 and state 2 are shown in Fig. 12. The dominant thermal emission process for both states is to the conduction band. The rates of the two states are very similar. Consequently, when a sample of *n*-type GaP:O is observed with a Schottky barrier by the DLTS method,²⁸ a single electron emission peak is observed. The method of measurement of the two rates and their analysis is de-

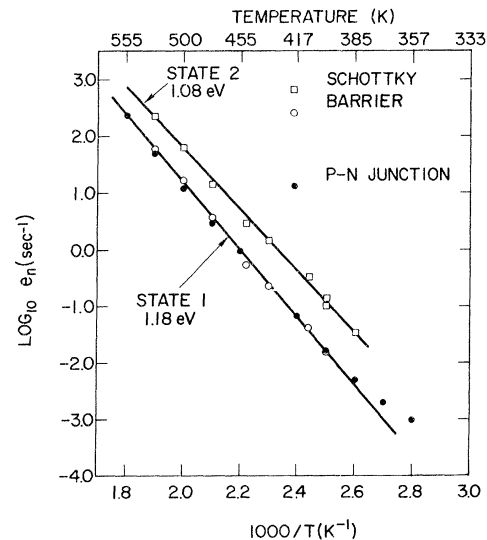


FIG. 12. Thermal emission rates of state 1 and state 2 of O in GaP. The activation energies 1.08 and 1.18 eV are larger than the binding energies E_{o1} and E_{o2} of state 1 and state 2. To determine E_{oi} , the contributions to the activation energy made by the temperature dependence of $N_c \sigma_{ni} \langle v_n \rangle$ must be subtracted out, $i = 1, 2$, where σ_{ni} is the capture cross section for the inverse of the thermal emission process.

scribed in Appendix B. A thermal activation energy $E_{02} = 0.89 \pm 0.06$ eV is deduced for state 2. This energy determines energy E_0 in Fig. 5(b). Examination of Fig. 5(b) shows that, in the absence of lattice frequency changes, E_0 should be the mean of the vertical separation of the levels from the conduction band before and after occupation. That is $E_0 = \frac{1}{2}(E_g - E_p + E_n)$, which is 1.18 eV for state 2 at 400 K. The fact that the measured value E_{02} is 0.29 eV smaller than this can be accounted for by a reduction of the lattice frequency after capture.

A configuration-coordinate diagram for state 2 at $T = 400$ K is shown in Fig. 13. This diagram is consistent with the measured energies E_{p2} , E_{n2} , E_{02} and also with the measured capture cross sections, discussed in Sec. IV D. The experimental and theoretical parameters are tabulated in Table II. At 400 K the calculated second moments are $(\langle E^2 \rangle_{n2})^{1/2} = 0.42$ eV and $(\langle E^2 \rangle_{p2})^{1/2} = 0.12$ eV. The experimental values are $(\langle E^2 \rangle_{n2})^{1/2} = 0.30$ eV and $(\langle E^2 \rangle_{p2})^{1/2} = 0.17$ eV. Thus the configuration-coordinate curve in Fig. 13 correctly predicts the large magnitude of the average second moment. The average of $(\langle E^2 \rangle)^{1/2} = \frac{1}{2}(0.12 + 0.42) = 0.27$ eV is in agreement with the measured value of $\frac{1}{2}(0.17 + 0.30) = 0.24$ eV. In contrast to these large values, the value of $(\langle E^2 \rangle)^{1/2}$ for the Zn-O center at the same temperature (400 K) is only 0.11 eV. While the overall

magnitude of $(\langle E^2 \rangle)^{1/2}$ is correct, the configuration-coordinate diagram predicts even a greater difference between the linewidths than the large difference actually observed.

D. Capture cross sections of state 2 of O in GaP

The qualitative but not quantitative fit of the linewidths makes it clear that we are trying to account for the complex phenomena of phonon-broadening and lattice relaxation with an extremely simple model and that we must allow for the fact that this model is not an exact description. Fortunately we can account for two unusual features of the capture cross sections of state 2 which will be insensitive to small changes in the configuration-coordinate diagram.

The first feature is the extremely large and temperature-independent cross section for the trapped electron to recombine with a hole ($\sigma_{p2} \approx 2 \times 10^{-14}$ cm²) despite the fact that this electron has an energy level in the upper half of the gap (i.e., $E_{02} = 0.89$ eV from thermal emission). This follows directly from the large lattice relaxation which causes the configuration-coordinate curve of the trapped electron to intersect the valence band close to the equilibrium position of the bound state.

The second feature is the small cross section (3×10^{-19} cm²) and small activation energy (0.11 eV) for capture of an electron into state 2. The trend of the other cases in Fig. 2 indicates that a cross section associated with this small an activation energy should be substantially larger. A possible explanation for the small cross section is that the configuration-coordinate diagram of the bound state does not intersect the conduction band (Fig. 13). The lack of intersection greatly reduces the capture cross section. The extent of this reduction is quite sensitive to just how close the configuration-coordinate curves come to intersecting. Therefore a quantitative calculation of σ_{n2} is very sensitive to the configuration-coordinate diagram parameters and it is misleading to claim agreement between theory and experiment, however, it is clear how a small cross section with small activation energy could arise. The configuration-coordinate diagram parameters, found by optical and thermal emission experiments and used to construct Fig. 13, are consistent with the lack of an intersection.

The large cross section for hole recombination σ_{p2} and the small cross section for electron capture σ_{n2} both result from a nonlinearity in E_t vs Q which enhances hole recombination and decreases electron capture. For the case of state 2 of O, these nonlinearities are established from the experimental determination of the configuration-coordinate diagram, discussed in Sec. IV C.

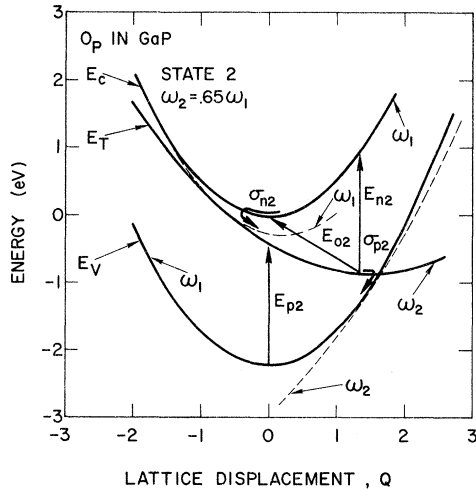


FIG. 13. Configuration coordinate diagram for state 2 of O in GaP. The diagram was determined by measurement of E_{p2} , E_{n2} , and E_{02} . The quantities ω_1 and ω_2 are the vibrational frequencies of the lattice before and after state 2 is occupied by an electron. The dashed curves are used to calculate capture cross sections with the theory of Sec. III, which did not take into account changes in lattice frequency. The dashed curve is a fit of the configuration-coordinate curve of the transition, in the region where capture takes place, with a curve having the same frequency as the initial state.

E. Configuration-coordinate diagram and analysis of hole capture by state 1 of O in GaP

In contrast to state 2, state 1 of O in GaP shows little lattice relaxation. One would not expect that such a deep center ($E_{01} = 0.896$ eV at low temperature) having little lattice relaxation would either capture electrons or holes by the MPE process. The electron capture cross section $\sigma_n \approx 2 \times 10^{-18}$ cm² varies slowly with temperature up to $T = 580$ K and therefore shows no evidence of MPE capture. Hole recombination is radiative at room temperature, but when the temperature increases above 450 K the cross section rapidly increases with an activation energy of $E_{\text{act}} = 0.56$ eV and the recombination becomes nonradiative, indicating that MPE capture has become dominant. At 526 K the MPE cross section is $\sigma_{p1} = (6 \pm 2) \times 10^{-21}$ cm².

The configuration coordinate diagram for state 1 of O is most accurately fit with luminescence data. Using the known binding energy $E_{01} = 0.896$ eV and assuming this energy scales with the energy gap at higher temperatures and using $S\hbar\omega \approx 0.09$ eV as determined from the separation of the first moment and zero phonon line of the capture⁷¹ and recombination⁷² luminescence bands at low temperature, we can calculate $f(0)$ and $\sigma_{p1} = Af(0)$. We will assume here that A is the same magnitude as calculated in Sec. III, although A may be somewhat different (perhaps by 1 order of magnitude) because the valence band and the deep level have different symmetries. We find $\sigma_{p1}^{\text{th}} = (1-8) \times 10^{-23}$ cm² and $E_{\text{act}}^{\text{th}} = 0.76$ eV. The cross section is 12 orders of magnitude too small to agree with experiment.

A reduction in the vibrational frequency after capture will greatly alter the point at which the trapped electron configuration-coordinate curve crosses into the the valence band and greatly increase σ_{p1} . Figure 14 shows the calculated configuration-coordinate diagram for state 1 of O at a temperature of 526 K, assuming $\omega_2 = 0.78\omega_1$. For this case $\sigma_{p1}^{\text{th}} = (1-12) \times 10^{-21}$ cm² and $E_{\text{act}}^{\text{th}} = 0.46$ eV are in rough agreement with experiment. This decrease in lattice frequency is evidence for a substantial nonlinearity in $E_t(Q)$ which enhances hole recombination and decreases electron capture.

Recently, Kopylov and Pikhtin⁷³ have analyzed the phonon broadening of the σ_p^0 optical cross section of the O donor. They find a Franck-Condon shift of $S\hbar\omega = 0.09$ eV in agreement with our own evaluation. However they find a value of $E_{01} = 0.89 \pm 0.02$ at $T = 300$ K, indicating that the O donor level remains fixed relative to the conduction band. In this case the separation of the O level and the valence band will decrease with temperature and consequently the cross-section data can be fitted

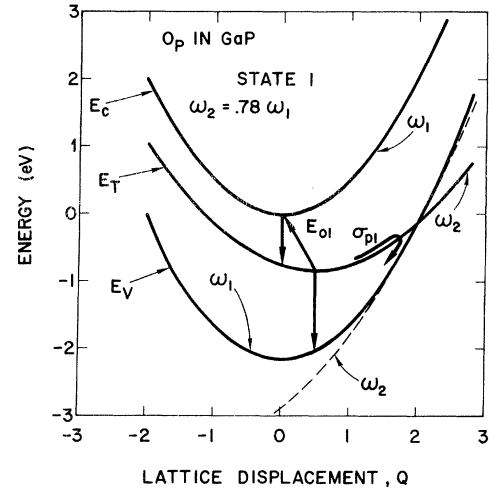


FIG. 14. Configuration-coordinate diagram for state 1 of O in GaP. The diagram was constructed from luminescence spectra of the two transitions indicated by the vertical arrows. The reduction in lattice frequency when the level is occupied $\omega_2 = 0.78\omega_1$ was adjusted to fit the σ_{p1} capture cross section. The MPE contribution to σ_{n1} is small and has not been measured.

with a slightly smaller lattice frequency change ($\omega_2 = 0.80\omega_1$).

V. SUMMARY

Evidence is presented that multiphonon emission (MPE) is commonly occurring in the capture of carriers by deep levels in GaP and GaAs. The magnitudes and temperature dependence of nine capture cross sections of impurities in GaAs and four capture cross sections of impurities in GaP can be interpreted as being due to MPE. The high-temperature behavior of these cross sections is $\sigma = \sigma_\infty e^{-E_\infty/kT}$, where $\sigma_\infty = 10^{-15} - 10^{-14}$ cm². A few other capture cross sections that were measured could not be interpreted in terms of MPE.

Large lattice relaxation of the bound state is necessary for sizeable MPE capture cross sections. Optical and thermal emission data for the Zn-O center and for the two-electron state of O in GaP showed that the lattice relaxation was adequate in these cases to account for the large electron-capture cross section of the Zn-O center and the large hole-capture cross section of the O center.

The only other likely nonradiative capture mechanism is the Auger effect. Auger capture is ruled out for three of the 13 cross sections studied.

Data for the Zn-O center and the one- and two-electron states O center in GaP, provide evidence that nonlinear behavior of the bound-state energy levels with lattice displacement strongly affects

the magnitudes of the MPE capture cross sections. In all cases the nonlinearities tended to increase hole recombination cross sections and to decrease electron-capture cross sections.

A detailed theory is presented for the capture of an electron from the conduction band by an attractive neutral center coupled to a single vibrational coordinate. A general formula for the capture cross section is derived with the lattice quantized and also treating the lattice classically. The calculation with the classical lattice clarified that capture transitions result from the crossing of the free and bound levels as the lattice vibrates, that the adiabatic approximation breaks down when the levels are separated by less than ≈ 0.06 eV and that the transitions take place while the levels are within this energy separation.

The capture cross section was related to the lattice relaxation parameters by first associating it with the phonon broadened line shape for radiative capture. (This relation had been made previously by other authors.)

The magnitude of the cross section is calculated using a spherical square-well model for the impurity. It is found that the capture cross section is independent of the range and depth of the well and insensitive to the energy-level separation at which the adiabatic approximation is estimated to break down. A rough calculation showed that about one-half the time, the captured carrier is reemitted into another conduction-band level before the lattice relaxes. The theory predicted the same order of magnitude for σ_{∞} as found experimentally. However, much of the data for σ_{∞} involved complexities not covered by the theory, such as charged centers and bound and free states of different symmetries.

The simple square-well model also predicts nonlinearities in the bound-state energy versus lattice displacement that are in qualitative agreement with the evidence for such nonlinearities.

ACKNOWLEDGMENTS

We thank A. Baldereschi, G. A. Baraff, J. J. Hopfield, M. Lax, M. Schlüter, and M. D. Sturge for helpful theoretical discussions. We are grateful to R. A. Logan for providing many GaAs samples and to F. R. Merritt and A. J. Williams for skillful experimental assistance.

APPENDIX A: MEASUREMENT OF THE OPTICAL CROSS SECTIONS FOR STATE 1 AND STATE 2 OF O IN GaP BY PHOTOCAPACITANCE EXPERIMENTS

The four optical cross sections σ_{p1}^0 , σ_{n1}^0 , σ_{p2}^0 , and σ_{n2}^0 are defined by the inserted diagrams in Figs. 10 and 11. The rate equations coupling state 1 and

state 2, with densities n_1 and n_2 follow from the insert diagram in Fig. 10(a),

$$\dot{n}_1 = [\sigma_{p1}^0 n_0 + \sigma_{n2}^0 n_2 - (\sigma_{n1}^0 + \sigma_{p2}^0) n_1] F, \quad (A1)$$

$$\dot{n}_2 = (\sigma_{p2}^0 n_1 - \sigma_{n2}^0 n_2) F, \quad (A2)$$

where

$$n_0 + n_1 + n_2 = N. \quad (A3)$$

n_0 is the density of the O center with no bound electrons, N is the total density of the O center, and F is the photon flux.

The coupled equations normally make the determination of the optical cross sections very complex. We have succeeded in simplifying the determination of these cross sections by modifying the original methods used by Kukimoto *et al.*²⁵ in two ways. First we apply a repetitive bias pulse which prepares the center in a particular charge state. Second, using a double boxcar integrator triggered by this pulse, we measure the light-induced capacitance change that occurs during a short time $\Delta t = 1$ msec after the pulse. The time interval is made short enough so that the changes in capacitance are linear in Δt . The change in capacitance ΔC is proportional to the change $\Delta n_1 + 2\Delta n_2$ that occurs during Δt . (The factor of 2 is because state 2 is doubly charged.)

For example, an injection pulse will saturate state 1 causing $n_1 = N$, $n_0 = n_2 = 0$. After the pulse the capacitance will change linearly with time due to the photoionization of state 1 and the filling of state 2. The capacitance change following the injection pulse is $\Delta C \sim 2\Delta n_2 + \Delta n_1 \sim (\sigma_{p2}^0 - \sigma_{n1}^0) F \Delta t$, where F is the photon flux. After a time of $\Delta t = 1$ msec following the injection pulse a 100-nsec recombination pulse is applied. This pulse causes recombination of one of the electrons in state 2, leaving the other electron in state 1. After the recombination pulse ΔC is $\propto -\sigma_{n1}^0 F \Delta t$ and the change in ΔC is $\propto \sigma_{p2}^0 F \Delta t$. Thus σ_{n1}^0 and σ_{p2}^0 may be measured directly by measuring ΔC with a double boxcar integrator. Similarly after a long recombination pulse $n_0 = N$ and $n_1 = n_2 = 0$. The light excites electrons from the valence band into the one-electron state giving a capacitance change $\Delta C \sim \sigma_{p1}^0 F \Delta t$. In this way the relative optical cross sections σ_{n1}^0 , σ_{p1}^0 , and σ_{p2}^0 shown in Fig. 10 were measured as a function of energy and temperature.

The remaining cross section σ_{n2}^0 was measured in a similar way using a transparent Au-Cr Schottky barrier on n -type GaP doped with O. The barrier normally had a reverse bias of 8 V. The barrier was repetitively pulsed to zero bias, filling state 2 and establishing $n_0 = n_1 = 0$ and $n_2 = N$. The light induced capacitance change is $\Delta C \sim \sigma_{n2}^0 F \Delta t$. This method was adequate for measuring σ_{n2}^0 over the first decade. However contributions to

ΔC due to other impurities in the sample with much smaller concentrations, but with lower threshold energies for photoionization than state 2 of O, interfered with the measurement of σ_{n2}^0 over many decades. Grimmeiss *et al.*⁶⁹ had measured the threshold of σ_{n2} over five decades. In order to measure σ_{n2}^0 over a similar range we gave up measuring σ_{n2}^0 by this method and instead measured σ_{n2}^0 by recording the complete exponential decay of the capacitance signal after filling state 2. This method is discussed by Kukimoto *et al.*²⁵ The photoionization of state 2 leaves an electron in state 1. The illumination of the sample is adjusted to insure that the electron in state 1 is also photoionized and at a rate that is rapid compared to state 2. Then the decay of the capacitance signal is a single exponential $\Delta C \sim e^{-\sigma_{n2}^0 F t}$. The exponential decay was recorded over a range of one to two decades using a Nicolet signal averager and a log amplifier. Other impurities present in low concentrations only affect a small portion of the initial decay. This portion of the decay was neglected in determining the decay rate. In this way σ_{n2}^0 was measured using both the Schottky barrier and also the p - n junction. In the case of the p - n junction, state 2 was filled by illuminating partially the sample at 1.8 eV. The data shown in Fig. 11 was measured over a range of up to five orders of magnitude. The cross section drops off smoothly with decreasing energy in a manner consistent with a phonon broadened line shape for photoionization of an electron nearly 2.0 eV below the conduction band. None of the structure and low-energy thresholds reported by Grimmeiss *et al.*⁶⁹ are observed. This structure may be due to small concentrations of extraneous impurities in their sample. Their photoconductivity method is sensitive to small concentrations of impurities in the sample having low-energy photoionization thresholds, just as our first method of measurement employing repetitive pulsing is.

The threshold energies E_{p2} and E_{n2} shown in the diagram in Fig. 11 can be determined from the optical cross sections. Broadening of the optical cross sections by lattice vibrations produces optical cross sections with a Gaussian tail. The cross sections can be fitted with

$$\sigma(E)/\sigma_{\max} = \exp\left\{-\left[\frac{(E - \bar{E})^2}{2\langle E^2 \rangle}\right]\right\}. \quad (\text{A4})$$

Kukimoto *et al.*²⁵ have discussed a simple model of the phonon broadening of an absorption edge. Their calculation is illustrated in Fig. 7 of Ref. 25. The unbroadened absorption edge near threshold has the form $\sigma \propto (E - E_t)^{1/2}$. Phonon broadening changes the abrupt square-root absorption edge into a Gaussian tail described by Eq. (A4), where

$$E_t \approx \bar{E} - \frac{1}{2}\langle E^2 \rangle^{1/2}. \quad (\text{A5})$$

We use this Eq. (A5) to determine E_{n2} and E_{p2} in Table II.

If the broadening is due to lattice vibrations, we expect that $\langle E^2 \rangle$ will be proportional to T at high temperatures and change substantially with temperature. This is the case for the cross sections associated with state 2. The parameters for these cross sections are tabulated in Table II.

The measured activation energies 1.18 and 1.08 eV are much larger than those previously measured by Kukimoto *et al.*²⁵ (0.78 eV for e_{n1} and 0.76 eV for e_{n2}). The previous measurements were only made in the temperature range $1000/T = 2.4$ – 2.8 . The data in Fig. 11 clearly indicates a smaller activation energy over this temperature range for σ_{n1} . It is possible that, at low temperatures, temperature-independent emission due to field ionization of the bound carriers is significant and acts to reduce the activation energies.

The large activation energy for state 1 $E_{th} = 1.14 \pm 0.06$ eV is puzzling. An activation energy somewhat less than the binding energy at low temperature (accurately known to be 0.896 eV) was expected. The capture cross section for state 1 does not increase with temperature and its magnitude is only $(1-2) \times 10^{-18}$ cm², so that it is probably not due to MPE. This capture process is thought to be non-radiative and is very likely due to an Auger mechanism. This effect could mask weaker MPE capture which is likely to be thermally activated.

APPENDIX B: MEASUREMENTS OF THE THERMAL EMISSION RATES OF STATE 1 AND STATE 2 AND THEIR INTERPRETATION

The thermal emission rates for state 1 and state 2, e_{n1} and e_{n2} , are plotted in Fig. 12. They were measured by populating state 2 by pulsing a Schottky barrier on n -type GaP:O with a 1-V quiescent bias to zero bias. The capacitance change first decays with rate e_{n2} , which is the faster of the two rates. The later part of the transient decays at rate e_{n1} . The two rates are sufficiently different to allow e_{n1} and e_{n2} to be separately determined. Rate e_{n1} was also measured using a p - n junction. Forward biasing the junction fills state 1. After the pulse, the electrons are emitted at rate e_{n1} . As shown in Fig. 12, the measurements on the Schottky barrier and the p - n junction give exactly the same rate e_{n1} versus temperature.

The activation energies we obtain are 1.18 eV for state 1 and 1.08 eV for state 2. The product $N\langle v \rangle$ is proportional to T^2 . Correcting the observed activation energies for this temperature

dependence reduces them each by $2kT \approx 0.08$ eV. The capture cross sections are temperature dependent and characterized by activation energies of -0.04 eV for σ_{n1} and $+0.11$ eV for σ_{n2} . Correcting for these temperature dependences and esti-

imating an overall error of ± 0.06 eV we find the two thermal activation energies to be

$$E_{01} = 1.14 \pm 0.06 \text{ eV,}$$

$$E_{02} = 0.89 \pm 0.06 \text{ eV.}$$

- ¹P. T. Landsberg, *Phys. Status Solidi* **41**, 457 (1970).
²P. T. Landsberg, *J. Lumin.* **7**, 3 (1973).
³K. Huang and A. Rhys, *Proc. R. Soc. A* **204**, 406 (1950).
⁴H. Gummel and M. Lax, *Phys. Rev.* **97**, 1469 (1955).
⁵R. Kubo and I. Toyazawa, *Prog. Theor. Phys.* **13**, 160 (1955).
⁶G. Richayzen, *Proc. R. Soc. A* **241**, 480 (1957).
⁷V. A. Kovarskii, *Fiz. Tverd. Tela* **4**, 1636 (1962) [*Sov. Phys.-Solid State* **4**, 1200 (1962)]; V. A. Kovarskii and E. P. Sinyavskii, *Fiz. Tverd. Tela* **4**, 3202 (1962); **6**, 636 (1964) [*Sov. Phys.-Solid State* **4**, 2345 (1963); **6**, 498 (1964)].
⁸E. P. Sinyavskii and V. A. Kovarskii, *Fiz. Tverd. Tela* **9**, 1464 (1966) [*Sov. Phys.-Solid State* **9**, 1142 (1967)].
⁹M. Lax, *Phys. Rev.* **119**, 1502 (1960).
¹⁰E. F. Smith and P. T. Landsberg, *J. Phys. Chem. Solids* **27**, 1727 (1966).
¹¹H. I. Ralph and F. D. Hughes, *Solid State Commun.* **9**, 1477 (1971).
¹²V. L. Bonch-Bruevich and V. B. Glasko, *Fiz. Tverd. Tela* **4**, 510 (1962) [*Sov. Phys.-Solid State* **4**, 371 (1962)].
¹³D. F. Nelson, J. D. Cuthbert, P. J. Dean, and G. D. Thomas, *Phys. Rev. Lett.* **17**, 1262 (1966).
¹⁴P. J. Dean, R. A. Faulkner, S. Kimura, and M. Ilegems, *Phys. Rev. B* **4**, 1926 (1971).
¹⁵J. S. Jayson, R. N. Bhargava, and R. W. Dixon, *J. Appl. Phys.* **41**, 4972 (1970); see also C. H. Henry, R. Z. Bachrach and N. E. Schumaker, *Phys. Rev. B* **8**, 4761 (1973).
¹⁶The room-temperature cross sections for exciton Auger recombination were estimated from the exciton Auger lifetime τ_{ex} and exciton binding energy E_{ex} . For recombination of holes at excitons bound to donors in *n*-type material

$$\sigma_p = \langle v_p \rangle \tau_{ex}^{-1} (n/N_c N_v) (g_{ex}/g_D) e^{E_{ex}/kT},$$
etc. For the capture of holes at the Zn-O center, the cross section was computed using the estimated Auger lifetime T_A for a hole concentration of $10^{18}/\text{cm}^3$:

$$\sigma_p = \langle v_p \rangle p T_A^{-1}.$$
¹⁷The Auger effect increases for deep centers because the deeply bound carrier has a higher probability of having the large momentum that is transferred to the carrier excited in the Auger effect. The most favorable situation would be a center which deeply binds two carriers thereby giving a large carrier density near the trap. See M. K. Sheinkman, *Fiz. Tverd. Tela* **7**, 28 (1965) [*Sov. Phys.-Solid State* **7**, 18 (1965)].
¹⁸E. W. Williams, *Phys. Rev.* **9**, 279 (1971).
¹⁹C. J. Hwang, *Phys. Rev.* **180**, 827 (1969).
²⁰For example, P. D. Dapkus, W. A. Hackett, Jr., O. G. Lorimor, and R. Z. Bachrach, *J. Appl. Phys.* **45**, 4920 (1974).
²¹A. A. Bergh and P. J. Dean, *Proc. IEEE* **60**, 156 (1972).
²²The capacitance transient technique was first used by R. Williams, *J. Appl. Phys.* **37**, 3411 (1966).
²³A comprehensive treatment of the study of deep levels by capacitance and current transients is given by C. T. Sah, L. Forbes, L. L. Rosier, and A. F. Tasch, Jr., *Solid State Electron.* **13**, 759 (1970).
²⁴C. T. Sah, W. W. Chan, H. S. Fu, and J. W. Walker, *Appl. Phys. Lett.* **20**, 193 (1972).
²⁵H. Kukimoto, C. H. Henry, and F. R. Merritt, *Phys. Rev. B* **7**, 2486 (1973).
²⁶C. H. Henry, H. Kukimoto, G. L. Miller, and F. R. Merritt, *Phys. Rev. B* **7**, 2499 (1973).
²⁷D. V. Lang, *J. Appl. Phys.* **45**, 3014 (1974).
²⁸D. V. Lang, *J. Appl. Phys.* **45**, 3023 (1974).
²⁹D. L. Losee, *Appl. Phys. Lett.* **21**, 54 (1972).
³⁰M. Schulz, *Appl. Phys.* **4**, 91 (1974).
³¹C. H. Henry and D. V. Lang, in *Proceedings of the Twelfth International Conference on the Physics of Semiconductors, Stuttgart, Germany*, edited by M. H. Pilkuhn (Teubner, Stuttgart, 1974), p. 411.
³²D. V. Lang and C. H. Henry, *Phys. Rev. Lett.* **35**, 1525 (1975).
³³C. H. Henry (unpublished).
³⁴D. V. Lang and R. A. Logan, *J. Electron. Mater.* **4**, 1053 (1975).
³⁵D. V. Lang and L. C. Kimerling, *Phys. Rev. Lett.* **33**, 489 (1974).
³⁶L. C. Kimerling and D. V. Lang, *Lattice Defects in Semiconductors 1974* (Institute of Physics, London, 1975), p. 589.
³⁷D. V. Lang and L. C. Kimerling, *Appl. Phys. Lett.* **28**, 248 (1976).
³⁸J. D. Weeks, J. C. Tully, and L. C. Kimerling, *Phys. Rev. B* **12**, 3286 (1975).
³⁹P. T. Landsberg, *Phys. Status Solidi* **41**, 457 (1970).
⁴⁰A. Haug, *Festkoerperprobleme XIII*, 411 (1972).
⁴¹A. A. Bergh and P. J. Dean, *Proc. IEEE* **60**, 156 (1972), p. 196.
⁴²A. G. Milnes, *Deep Impurities in Semiconductors* (Wiley, New York, 1973), Chap. 5.
⁴³H. J. Queisser and U. Heim, *Ann. Rev. Mater. Sci.* **4**, 125 (1974).
⁴⁴M. Lax, *J. Chem. Phys.* **20**, 1752 (1952).
⁴⁵L. D. Landau and E. M. Lifshitz, *Quantum Mechanics* (Addison-Wesley, Reading, Mass., 1958), p. 310.
⁴⁶C. Zener, *Proc. R. Soc. A* **137**, 696 (1932).
⁴⁷G. L. Miller, *IEEE Trans. Electron Devices* **ED-19**, 1103 (1972).
⁴⁸J. S. Jayson, R. Z. Bachrach, P. D. Dapkus, and N. E. Schumaker, *Phys. Rev. B* **6**, 2357 (1972).
⁴⁹R. R. Senchal and J. Basinski, *J. Appl. Phys.* **39**, 4581 (1968).
⁵⁰J. C. Carballes and J. Lebailly, *Solid State Commun.* **6**, 167 (1968).
⁵¹M. Bleicher and E. Lange, *Solid-State Electron.* **16**,

- 375 (1973).
- ⁵²F. Hasegawa, *Jpn. J. Appl. Phys.* **9**, 638 (1970).
- ⁵³F. D. Hughes, *Acta Electron.* **15**, 43 (1972).
- ⁵⁴H. Okamoto, S. Sakta, and K. Sakai, *J. Appl. Phys.* **44**, 1316 (1973).
- ⁵⁵G. H. Glover, *IEEE Trans. Electron Devices* **ED-19**, 138 (1972).
- ⁵⁶Reference 36, Chap. 3.
- ⁵⁷D. L. Dexter, in *Solid State Physics*, edited by F. Seitz and D. Turnbull (Academic, New York, 1958), Vol. 6, p. 358.
- ⁵⁸J. J. Markham, in *Solid State Physics*, edited by F. Seitz and D. Turnbull (Academic, New York, 1966), Suppl. 8, p. 370.
- ⁵⁹R. Engleman and J. Jortner, *Mol. Phys.* **18**, 145 (1970).
- ⁶⁰W. H. Fonger and C. W. Struck, *J. Lumin.* **8**, 452 (1974).
- ⁶¹*Bateman Manuscript Project, Higher Transcendental Functions*, edited by A. Erdelyi (McGraw-Hill, New York, 1953), Vol. II, p. 86.
- ⁶²G. F. Koster, J. O. Dimmock, R. G. Wheeler, and H. Stotz, *Properties of the 32 Point Groups* (MIT, Cambridge, Mass., 1963), p. 89.
- ⁶³C. H. Henry, P. J. Dean, and J. D. Cuthbert, *Phys. Rev.* **166**, 754 (1968).
- ⁶⁴E. Cohen, M. D. Sturidge, N. O. Lipori, M. Altarelli, and A. Baldereschi, *Phys. Rev. Lett.* **35**, 1593 (1975).
- ⁶⁵V. Heine and C. H. Henry, *Phys. Rev.* **11**, 3795 (1975).
- ⁶⁶J. D. Cuthbert, C. H. Henry, and P. J. Dean, *Phys. Rev.* **170**, 739 (1968).
- ⁶⁷T. N. Morgan, M. H. Pilkuhn, and M. R. Lorentz, *Proceedings of the International Conference on Luminescence, Budapest, Hungary, 1966* (unpublished).
- ⁶⁸Cross section σ_{n1}^0 measured by Kukimoto *et al.* (Ref. 25) was in error, consequently these data did not agree with measurements of this cross section by Braun and Grimmeiss [*Solid State Commun.* **12**, 657 (1973)]. Our new data for σ_{n1} agree with that of Braun and Grimmeiss. This error had to do with the shape of σ_{n1}^0 . It did not affect the determination of the energy levels of state 1 and state 2. Our new measurements verify the findings of Kukimoto *et al.* (Ref. 25), that there is a large lattice relaxation associated with state 2.
- ⁶⁹H. Grimmeiss, L. A. Ledebor, C. Ovren, and T. N. Morgan, Ref. 31, p. 386.
- ⁷⁰M. Jaros, *J. Phys. C* **8**, 2455 (1975).
- ⁷¹P. J. Dean and C. H. Henry, *Phys. Rev.* **176**, 928 (1968).
- ⁷²P. J. Dean, C. H. Henry, and C. J. Frosch, *Phys. Rev.* **168**, 812 (1968).
- ⁷³A. A. Kopylo and A. N. Pikhtin, *Sov. Phys.-Semicond.* **8**, 1563 (1975).